NASA TECHNICAL MEMORANDUM

NASA TM X-949

NASA TM X-949

THE EXPLORER XVI MICROMETEOROID SATELLITE

SUPPLEMENT III, PRELIMINARY RESULTS FOR THE PERIOD MAY 27, 1963, THROUGH JULY 22, 1963

Compiled by Earl C. Hastings, Jr.

Langley Research Center
Langley Station, Hampton, Va.

NATIONAL AERONAUTICS AND SPACE ADMINISTRATION • WASHINGTON, D. C. • MARCH 1964

NASA Langley Research Center, Langley Station, Va.

THE EXPLORER XVI MICROMETEOROID SATELLITE

SUPPLEMENT III, PRELIMINARY RESULTS FOR THE PERIOD MAY 27, 1963, THROUGH JULY 22, 1963

Compiled by Earl C. Hastings, Jr.

Langley Research Center
Langley Station, Hampton, Va.

Washington, NASA, mar. 1964 38p ref

(NASA TM X-949) OTS: $1.00

NATIONAL AERONAUTICS AND SPACE ADMINISTRATION

For sale by the Office of Technical Services, Department of Commerce, Washington, D.C. 20230 -- Price $1.00

THE EXPLORER XVI MICROMETEOROID SATELLITE

SUPPLEMENT III, PRELIMINARY RESULTS FOR THE PERIOD MAY 27, 1963, THROUGH JULY 22, 1963

Compiled by Earl C. Hastings, Jr.
Langley Research Center

16692

A

SUMMARY

Both of the telemetry systems have ceased to transmit usable experimental data. The first telemeter system failed completely on May 29, 1963, and the second telemeter failed on July 22, 1963. Power supply systems were operating satisfactorily when these failures occurred, and telemetry temperatures were below design limits in both cases.

Through July 22, 1963, punctures were recorded in 44 of the 0.001-inch-thick beryllium-copper pressurized cells and in 11 of the 0.002-inch-thick beryllium-copper pressurized cells. Corresponding puncture rates are 0.031 and 0.016 puncture/sq ft/day, respectively. When expressed in equivalent thicknesses of aluminum, tne puncture rates still lie somewhat above the lower previous estimates for that material. No punctures of 0.005-inch-thick beryllium-copper cells have been recorded, and the upper average puncture rate limit with 95-percent confidence is 0.009 puncture/sq ft/day. One break of a 0.003-inch copper-wire card detector was indicated on June 28, 1963, and a break of a 0.002-inch copper-wire card detector was indicated on July 13, 1963.

Impact detector data through April 19, 1963, indicate higher impact rates than found in previous impact detector experiments. There appears to be some correlation of impact rate with rate of puncture of the pressurized cells.

AUTHOR

INTRODUCTION

The Explorer XVI (1962 Beta Chi 1) micrometeoroid satellite (fig. 1) was described in reference 1, and some data and an analysis were presented for the first 4 weeks in orbit. Reference 2 was the first supplement to that initial report and extended the period covered through March 2, 1963. Reference 3, the second supplement, extended the period covered through May 26, 1963, discussed a partial failure of telemeter A, and provided some statistical studies of the puncture data. The present report is the last supplement, extending the period covered through July 22, 1963, which was the last day on which usable experimental data were received from the satellite.

The report presents puncture data from the pressurized-cell and copper-wire card experiments. Impact detector data for the period between December 16, 1962, and April 19, 1963, are also presented and compared with the pressurized-cell puncture data and with impact detector data from previous experiments. Also included are a discussion of the telemeter failures, brief descriptions of the power supply system and the data reduction method, and some data and discussion concerning satellite temperatures.

The names and organizations of the experimenters and specialists who have contributed to this report are given in the following list:

Contributor	Contribution
Jose M. Alvarez Langley Research Center	Statistical Curve Fit for Pressurized-Cell Experiment
Alfred G. Beswick Langley Research Center	Impact Detection Systems
Charles A. Gurtler Langley Research Center	Pressurized-Cell Experiment
Sheldon Kopelson Langley Research Center	Data Reduction
Wendell H. Lee Langley Research Center	Temperatures
Walt C. Long Langley Research Center	Telemetry Performance
John L. Patterson Langley Research Center	Power-Supply-System Performance
Luc Secretan Goddard Space Flight Center	Copper-Wire Card Detectors Cadmium Sulfide Cells

TELEMETRY PERFORMANCE

Both telemeters on the Explorer XVI satellite have ceased transmitting usable data. Telemeter A had suffered a shorted commutating transistor on April 20, 1963, as reported in reference 3. On May 29, 1963, some time between passes 2,260 and 2,264, the same telemeter suffered a second failure which effectively ended its usefulness. On or about July 22, 1963, between passes 3,013 and 3,019, telemeter B experienced a failure which ended its usefulness. An analysis has been made of the various failures and although no definite conclusions can be drawn at this time as to the nature of the failures, the effects of these failures on the data received, and the tentative results of the studies can be discussed.

The telemeter A records on and after pass 2,264 on May 29, 1963, showed that the signal had ceased pulsing and consisted of a single continuous tone for the duration of the interrogation. It is inferred that the telemeter encoder had ceased commutating and was stuck on one channel. Of the 64 records examined, 27 were of one test solar cell and 11 were of a different test solar cell. (A solar cell record is recognized by its characteristic half-rectified sine-wave form due to satellite spin.) Three of these records contained multiple interrogations with different test solar cells on during subsequent interrogations. On pass 2,573 the telemeter came on with one test solar cell, switched off and then on with a different test solar cell, off, and then on again with the first solar cell. In ground tests with an identical encoder, the observed behavior of telemeter A after May 29, 1963, could be duplicated by simulating two types of failures: a collector-to-emitter short in a transistor in the encoder Royer circuit (the low-frequency subcarrier oscillator used to generate the duration and space times) or a loss of the -3.9-volt direct-current bias from the d-c to d-c converter. Yet neither of these fully explains the observations. In all of the records examined to date, none give any indication of being on a channel which is not a test solar cell. There are only five test solar cells and a total of 16 channels. When the satellite is interrogated, the scale-of-sixteen counter and the switching matrix can start on any one of the 16 channels. Although there is some preference for a particular channel, there should be no marked preference for test solar cells as has been observed. The fact that the channels were from different test solar cells makes the possibility of a failure in the scale-of-sixteen counter and the switching matrix highly unlikely.

On or about pass 2,916 on July 15, 1963, the telemeter A video signals changed from a sinusoidal form to a highly distorted signal. The effect on the data was as if the subcarrier oscillator had become quite noisy. However, scrutiny of the individual oscillations of the video signals showed that the sinusoidal oscillation was missing half-cycles, then whole cycles, and eventually whole groups of cycles. This last type of signal is characteristic of that available from a blocking oscillator.

Telemeter B performed satisfactorily through pass 3,005 on July 22, 1963, but failed sometime between passes 3,013 and 3,019. Thereafter the telemetry signals were subcarrier oscillator bursts wherein the duration and space times were abnormally short (less than 1 millisecond instead of more than 4 milliseconds). The subcarrier oscillator bursts were all of the same frequency, the duration times were all identical, and the space times were all identical.

Attempts have been made (using an identical pair of telemeters) to reproduce signals on the ground similar in waveform and nature to those received from Explorer XVI. Progressively decreasing the battery voltage far below design limits produced the singular results of not only duplicating the signals from Explorer XVI but also in the same order in which they had been observed to occur for both telemeter A and telemeter B. However, data from telemeter B through July 22, 1963, showed that the telemeter A battery voltage was well within design limits. In addition, radio-frequency-signal strength records for both telemeter A and telemeter B on August 31, 1963, and on September 25, 1963, show neither battery voltage to be below design limits. A more detailed discussion of power supply systems operation is presented in a following section.

As can be seen from the preceding discussion, the basic causes of the failures are not yet completely defined. It is clear, however, that none of the failures discussed can be attributed to the command receivers, the solar cells, the Ni-Cd batteries, or the transmitters.

PRESSURIZED-CELL EXPERIMENT

During the 7-month useful lifetime of Explorer XVI, the pressurized-cell experiment sustained one or more punctures in 44 of the one hundred 0.001-inch and 11 of the forty 0.002-inch beryllium-copper sensors. None of the twenty 0.005-inch beryllium-copper sensors were punctured.

Table I shows the first interrogation in which each new puncture was recorded and the elapsed time since the last previous interrogation for the time period May 27, 1963, through July 22, 1963.

TABLE I

Pass	Greenwich date	Greenwich mean time at interrogation	Time since last interrogation, hr	min	Accumulated punctures for detector thickness of -		
					0.001 in.	0.002 in.	0.005 in.
2,244	May 28, 1963	0327	3	49	39	10	0
2,260	May 29, 1963	0730	16	44	40	10	0
2,282	May 30, 1963	2256	9	19	41	10	0
2,383	June 7, 1963	0629	25	20	41	11	0
2,587	June 21, 1963	2359	6	59	42	11	0
2,655	June 26, 1963	2254	8	10	43	11	0
2,692	June 29, 1963	1516	10	29	44	11	0

The greatest uncertainty in the time of occurrence of a puncture was 25 hours and 20 minutes.

Table II shows a history of the 83 interrogations from which data were reduced during the time period of May 27, 1963, through July 22, 1963. Only three of these interrogations contain data from both telemeters, since useful data transmission from telemeter A ceased on May 29, 1963. The passes marked with an asterisk indicate the interrogations from which two telemetric transmissions were reducible.

TABLE II

Pass	Greenwich date	Greenwich mean time at interrogation	Accumulated punctures for detector thickness of -		
			0.001 in.	0.002 in.	0.005 in.
2,229	May 27, 1963	01:36	38	10	0
*2,238	May 27, 1963	18:29	38	10	0
2,241	May 27, 1963	23:38	38	10	0
*2,244	May 28, 1963	03:27	39	10	0
2,246	May 28, 1963	07:01	39	10	0
2,250	May 28, 1963	14:46	39	10	0
*2,260	May 29, 1963	07:30	40	10	0
2,264	May 29, 1963	15:10	40	10	0
2,277	May 30, 1963	13:37	40	10	0
2,282	May 30, 1963	22:56	41	10	0
2,285	May 31, 1963	02:45	41	10	0
2,291	May 31, 1963	14:04	41	10	0
2,297	May 31, 1963	23:49	41	10	0
2,299	June 1, 1963	03:17	41	10	0
2,301	June 1, 1963	06:48	41	10	0
2,310	June 1, 1963	23:42	41	10	0
2,312	June 2, 1963	02:01	41	10	0
2,318	June 2, 1963	12:59	41	10	0
2,324	June 3, 1963	00:07	41	10	0
2,326	June 3, 1963	02:05	41	10	0
2,328	June 3, 1963	05:43	41	10	0
2,338	June 3, 1963	23:06	41	10	0
2,342	June 4, 1963	06:15	41	10	0
2,355	June 5, 1963	04:38	41	10	0
2,359	June 5, 1963	12:16	41	10	0
2,369	June 6, 1963	05:09	41	10	0
2,383	June 7, 1963	06:29	41	11	0
2,396	June 8, 1963	03:55	41	11	0
2,410	June 9, 1963	04:27	41	11	0
2,419	June 9, 1963	21:12	41	11	0
2,425	June 10, 1963	06:29	41	11	0
2,427	June 10, 1963	10:29	41	11	0
2,437	June 11, 1963	03:53	41	11	0
2,467	June 13, 1963	07:44	41	11	0
2,473	June 13, 1963	19:01	41	11	0
2,481	June 14, 1963	08:13	41	11	0
2,495	June 15, 1963	08:38	41	11	0
2,500	June 15, 1963	17:56	41	11	0
2,507	June 16, 1963	05:04	41	11	0
2,522	June 17, 1963	07:31	41	11	0
2,528	June 17, 1963	18:42	41	11	0

*Interrogations from which two telemetric transmissions were reducible.

TABLE II - Concluded

Pass	Greenwich date	Greenwich mean time at interrogation	Accumulated punctures for detector thickness of -		
			0.001 in.	0.002 in.	0.005 in.
2,536	June 18, 1963	07:59	41	11	0
2,548	June 19, 1963	04:28	41	11	0
2,554	June 19, 1963	15:47	41	11	0
2,563	June 20, 1963	06:48	41	11	0
2,568	June 20, 1963	16:09	41	11	0
2,583	June 21, 1963	17:00	41	11	0
2,587	June 21, 1963	23:59	42	11	0
2,614	June 23, 1963	22:54	42	11	0
2,619	June 24, 1963	08:50	42	11	0
2,624	June 24, 1963	16:18	42	11	0
2,628	June 24, 1963	23:26	42	11	0
2,631	June 25, 1963	05:01	42	11	0
2,638	June 25, 1963	16:40	42	11	0
2,645	June 26, 1963	05:26	42	11	0
2,650	June 26, 1963	14:44	42	11	0
2,655	June 26, 1963	22:54	43	11	0
2,672	June 28, 1963	04:20	43	11	0
2,679	June 28, 1963	15:57	43	11	0
2,686	June 29, 1963	04:47	43	11	0
2,692	June 29, 1963	15:16	44	11	0
2,698	June 30, 1963	01:09	44	11	0
2,707	June 30, 1963	16:42	44	11	0
2,728	July 2, 1963	06:20	44	11	0
2,733	July 2, 1963	14:32	44	11	0
2,740	July 3, 1963	02:38	44	11	0
2,754	July 4, 1963	02:59	44	11	0
2,755	July 4, 1963	05:16	44	11	0
2,760	July 4, 1963	14:08	44	11	0
2,766	July 4, 1963	23:26	44	11	0
2,774	July 5, 1963	13:05	44	11	0
2,793	July 6, 1963	22:16	44	11	0
2,807	July 7, 1963	22:39	44	11	0
2,815	July 8, 1963	12:23	44	11	0
2,837	July 10, 1963	03:51	44	11	0
2,862	July 11, 1963	22:25	44	11	0
2,890	July 13, 1963	23:17	44	11	0
2,900	July 14, 1963	16:07	44	11	0
2,916	July 15, 1963	20:12	44	11	0
2,928	July 16, 1963	18:01	44	11	0
2,931	July 16, 1963	22:37	44	11	0
2,964	July 19, 1963	08:44	44	11	0
3,005	July 22, 1963	08:01	44	11	0

Table III shows the time-area products and puncture rates for the total lifetime of the experiment.

TABLE III

Material thickness, in.	Number of punctures	Time-area products for 218 days, sq ft-days	Puncture rate, punctures/sq ft/day
0.001	44	1,431	0.031
.002	11	682	.016
.005	0	405	

The total time-area product for the 0.001-inch sensors was 1,431 sq ft-days with an average puncture rate of 0.031 puncture/sq ft/day. This rate is very close to the previously reported rates of 0.035 based on 10 punctures, 0.034 based on 24 punctures, and 0.030 based on 38 punctures. (See refs. 1, 2, and 3.) The total time-area product for the 0.002-inch sensors was 682 sq ft-days with an average puncture rate of 0.016 puncture/sq ft/day. This rate is somewhat less than the previously reported rates of 0.020 based on 6 punctures and 0.017 based on 10 punctures.

Figure 2 shows three curves of predicted puncture rate as a function of thickness for aluminum sheet (from ref. 4). The puncture rates for the beryllium-copper, as shown in table III, have been converted to estimated puncture rates in aluminum sheet by considerations of the factor discussed in reference 1. The converted puncture rates, increased by 4/3 to correct for earth shielding (ref. 1) are shown in figure 2. The width of the bar extending through each point corresponds to the variation in thickness of the test material.

Confidence limits (confidence coefficient = 0.95) for the Explorer XVI data points plotted in figure 2 have been indicated in the figure. These limits were computed by using the χ^2 distribution in the manner described in the appendix of reference 3. The corrected form of expression (5) given on page 16 of reference 3 is

$$\frac{\chi^2_{\frac{\alpha}{2}}(2K)}{2T}, \quad \frac{\chi^2_{1-\frac{\alpha}{2}}(2K+2)}{2T}$$

for the confidence coefficient $(1 - \alpha)$, where K is number of pressurized cells punctured and T is total time-area product. These limits indicate that one can expect with 95-percent confidence that the puncture rate, in punctures/sq ft/day, will lie between 0.022 and 0.041 for 0.001-inch beryllium-copper, between 0.008 and 0.029 for 0.002-inch beryllium-copper, and between 0 and 0.009 for 0.005-inch beryllium-copper. The upper and lower puncture rates have been converted in the same manner as the observed puncture rates for plotting in figure 2.

The comparison shown in figure 2 has changed very little from the last previously reported comparison (ref. 3 - data to May 26, 1963). The puncture rate of the 0.001-inch sensors continues to be about $2\frac{1}{2}$ times greater than the value indicated by the lower curve, and the puncture rate for the 0.002-inch sensors is still relatively higher. These data indicate a more gradual decrease of puncture rate with increasing skin thickness than estimated for this range of thicknesses. The upper and lower confidence limits, however, are slightly closer to the observed value in view of the increased amount of data that have been obtained.

In reference 3 a maximum-likelihood curve of puncture rate against thickness was derived for the puncture data up to May 26. The parameters of this curve have been redetermined in order for the curve to correspond to all of the puncture data obtained. The equation of the new curve is

$$\psi = 0.724 \times 10^{-6}\tau^{-1.58}$$

where ψ is the puncture rate and τ is the thickness of the material in inches. Small variations in the nominal thicknesses of the pressure cells were investigated, and the average thicknesses of 0.00115, 0.00215, and 0.00515 inch were considered more realistic than 0.001, 0.002, and 0.005 inch, respectively. Hence, these average values were used in recalculating the equation which is plotted as the dashed line in figure 3.

COPPER-WIRE CARD DETECTORS

Telemeter A gave no indication of a break in either the 0.002-inch or the 0.003-inch copper wires on the card detectors, up to the time of its final failure. Telemeter B indicated a broken 0.003-inch wire on June 28, 1963, and a broken 0.002-inch wire on July 13, 1963.

CADMIUM SULFIDE CELLS

Analysis of penetration data from the two cadmium sulfide cells is being continued by Mr. Luc Secretan of the NASA Goddard Space Flight Center.

IMPACT DETECTION SYSTEMS

A meteoroid impact detection experiment employing the microphone technique as described in reference 1 was a part of the Explorer XVI satellite. The main purpose of the experiment was to measure meteoroid population in a momentum range, somewhat higher than that of previous such measurements, where few data exist. By partly bridging the gap between satellite and probe measurements and ground-based observations of meteor phenomena, such a measurement may improve

present knowledge of the relationships among meteoroid population, mass, and spacecraft skin penetrability. A secondary purpose was to provide more data for correlation with impact data previously obtained by other satellites.

Three levels of momentum sensitivity were provided for the impact detection systems. The low sensitivity was established as low as was practical, consistent with maintaining statistically adequate impact rates. The high sensitivity was chosen to approximate the lower sensitivities of other satellite impact detection experiments. The third sensitivity is intermediate between these two.

Figure 4 presents three estimates of the earth's meteoroid environment proposed by different observers (refs. 4 and 5), and shows the three thresholds of mass sensitivity of the Explorer XVI impact detection experiment. Particle impact velocity of 15 km/sec was assumed in assigning the Explorer XVI mass sensitivities. Table IV lists the momentum sensitivities and also the geometric areas exposed to meteoroid impact for each of the three levels of sensitivity.

TABLE IV

Size and shape	Area	Sensitivity
Nose-cone sounding boards, 410 stainless steel (2)		
Section of cone 12.5 cm wide 59.2 cm O.D. 32.8 cm I.D. 0.079 cm thick	Each: 709 sq cm (0.764 sq ft) Total: 1,418 sq cm (1.53 sq ft)	1.0 dyne-sec and 0.1 dyne-sec
Pressurized cells, beryllium-copper (20)		
Semicylindrical 18.8 cm long 4.93 cm diameter 0.0125 cm thick	Each: 92.8 sq cm (projected) Total: 1,856 sq cm (2.0 sq ft)	0.5 dyne-sec

The meteoroid impact detection systems of the Explorer XVI are of the threshold type; that is, only impacts above a certain momentum are recognized. Only impacts upon selected acoustically isolated surfaces of the satellite are recorded. Two different physical configurations of surfaces are employed. Two "sounding boards" located on the conical portion of the satellite nose (fig. 1) are used for the high and the low sensitivities, and the twenty 0.005-inch-thick pressurized-cell detectors are impact sensitized and used for the intermediate level.

Figure 5 is an exploded view of one of the impact sensing transducers used for the sounding boards and the pressure cells. The key element of the impact sensing transducer assembly of figure 5 is the lead zirconate titanate piezoelectric crystal. The voltage developed by this element as a result of the mechanical perturbation of an impact process is electrically isolated from the satellite structure by the quartz transfer and insulating disks. The cantilever spring holding clip applies a static loading to the element, optimized for a given assembly by adjusting the thickness of the brass dome nesting shim. The plastic holding collar prevents gross lateral movement of the assembly.

Each of the two sounding boards has a pair of impact sensing transducer assemblies mounted to its underside and electrically paralleled. Impact event signals from either sounding board are sent to an amplifier, which equalizes the effective sensitivity of the two sounding boards. The two sounding boards, in effect, thus function as one detector surface. The high- and low-sensitivity differentiation is made within the amplifier. The impact sensitizing of the 20 pressurized cells is accomplished by mounting the previously described sensing assembly to the underside of each pressurized cell, as described in reference 1.

Figure 6 is a block diagram of the impact detection system for the sounding boards; however, the pressurized-cell impact detection system is essentially the same. The mechanical perturbance produced by the impact of a meteoroid upon a detector surface travels throughout the surface and is intercepted by the piezoelectric element attached to the underside of the surface. The resulting signal is amplified, rectified, and filtered, and applied to a monostable multivibrator. If the peak amplitude of the signal at this point is sufficiently large, the multivibrator will be triggered, and will execute its cyclic excursion. It is here that the threshold decision is made; that is, signal amplitudes below the multivibrator trigger level will not be recognized, but greater amplitudes, no matter how large, will be accepted. The multivibrator pulse output is then applied to binary counterstorage. The accumulated stored count is transmitted whenever the satellite responds to an interrogation. The low-sensitivity signal selection is made within the amplifier by applying a one-tenth-amplitude signal sample of the detector surface transducer to a second multivibrator and counterstorage system. The counterstorage circuitry status is not disturbed by the interrogation-transmission process. Each counterstorage circuit has sufficient capacity such that recycling of the count does not occur more often than once a week.

The same calibration technique that has been employed for most previous U.S. satellite microphone-type impact detection experiments was applied to the Explorer XVI systems. The technique employs particles of known mass falling upon the detector surface through known heights, so that impact momenta are known. These momenta are corrected by application of the appropriate coefficient of restitution of the impact process. The calibration momenta are made equal to the anticipated momenta of impacting meteoroids, and it is assumed that the impact calibrations so obtained are valid for meteroid encounter, even though meteoroid velocities are enormously greater, and masses correspondingly smaller, than those of the particles used for calibration.

The particles employed in the calibration of the Explorer XVI impact detectors were synthetic sapphire spheres having masses from 130 micrograms to 16 milligrams. Calibration impact velocities ranged from 30 to 60 centimeters per second. Measured coefficients of restitution varied from 0.6 to 0.8 for impacts on the nose-cone sounding boards, and were about 0.3 for the impacts on the impact-sensitized pressurized-cell detectors. An average sensitivity for each detector surface was determined by impacting particles at a number of points on the surface, since the transducer response depends upon its distance from the impact point. Since temperatures and power supply voltages were expected to vary during flight, the calibration process also determined the effects of the anticipated variations on the response characteristics of the electronic portions of the impact detection systems.

Two of the three meteoroid impact detecting systems of the Explorer XVI satellite appeared to operate properly as indicated by the telemetry data reduced for the 125-day period from launch (December 16, 1962) through April 19, 1963. Figures 7, 8, and 9 present the variation with time of the counting rate of each of the three systems. Figure 7 shows the counting rate performance of the high-sensitivity impact detection system of the nose-cone sounding boards. The operational behavior of this system is peculiar in that the impact counting rate is very high during the first few days of the flight, and decreases rapidly with time. After the sixth day, the decrease of counting rate is less rapid, but not until the 31st day does this rate reach an apparently stable level, much lower than had been anticipated. At this time the counting rate closely approaches that of the low-sensitivity system, to which it is related through common detector surfaces, transducers, and portions of supporting electronics. The progressive reduction of counting rate and its stabilizing at a level much lower than expected has been assumed to indicate partial failure of the high-sensitivity impact detection system. Analysis of these data has accordingly been postponed pending further study, although some possible explanations are subsequently discussed herein.

Figure 8 shows the variation with time of the counting rate of the low-sensitivity impact detection system. This counting rate also decreases during the first month, although the rate of decrease is much less rapid than that of the high-sensitivity impact detection system. This system appears to be operating normally; however, its data have not yet been thoroughly studied.

Figure 9 presents the variation with time of the counting rate of the intermediate-sensitivity meteoroid impact detection system, which detects impacts on the 0.005-inch pressurized-cell detectors. The impacts detected by this system are considered to be most directly related to penetrations of the pressurized cells.

The data of figures 7, 8, and 9 are as received from the automatic data reduction of telemetry recordings. Corrections to these data due to satellite electronics package temperature and supply voltage fluctuations typical of orbital flight have been examined and found insignificant. However, other factors could affect these data, as will be discussed subsequently herein.

Figure 10 presents the number of impacts accumulated each day by the intermediate-sensitivity meteoroid impact detection system for the first

125 days of the Explorer XVI flight. Also shown in this figure is the history of the penetrations of the pressurized-cell detectors. The width of the symbols representing the penetrations indicates the time interval during which the penetration occurred; that is, the symbol width represents the time lapse between the successive data receptions which bracket the penetration event. It should be noted that figure 10 shows a daily impact accumulation even though data from the Explorer XVI were received at irregular intervals, sometimes several receptions per day and sometimes less than one per day. In preparing figure 10, the impact rate was assumed to be constant between successive data receptions.

Figure 10 indicates correlation between impact and penetration rates on the pressurized-cell experiments. For example, impact activity during the 21st- to 51st-day interval is about twice the arithmetic mean value of impact activity for the 125 days (indicated by the horizontal line of figure 10). During this 30-day interval 10 penetrations of 0.001-inch pressurized cells, and 4 penetrations of 0.002-inch pressurized cells were recorded. Penetrations were also recorded in the 102d- to 104th-day interval, 107th- to 110th-day interval, and other intervals concurrently with impact activities above the value of the mean. Conversely, when impact activity was low, penetrations usually occurred at minimum rates.

Figure 11 presents daily accumulation of impacts recorded by the Explorer XVI low-sensitivity meteoroid impact detection system. Comparison of this figure with the penetration history and the intermediate-system impact activity of figure 10 shows good correlation for most of the 125-day period. Thus, it is apparent that a relationship between penetration rates and impact rates exists. However, the numerical assessment of the correlation is difficult and not yet established with precision, as discussed subsequently.

Figure 12 shows summaries of the results from the Explorer XVI impact detecting systems superimposed upon proposed models of the earth's meteoroid environment. The equivalent mass sensitivities of the impact detecting systems were derived by assuming that the observed momentum response of the systems during calibration is valid during meteoroid encounter, as previously discussed, and by assuming that the average velocity of impacting meteoroids is 15 km/sec. The points located on the vertical lines representing the performance of the three impact detection systems are the values of arithmetic mean for the 120-day interval, the first 5 days being excluded. The ends of the lines indicate the highest and lowest 5-day average counting rates achieved during the period.

Figure 12 also shows the influx rate of meteoroid particles capable of penetrating the 0.001- and 0.002-inch detectors, taken from the material as previously discussed and presented in figure 2. In order to construct figure 12, the effective mass sensitivities of the pressurized-cell detectors were determined by application of the hypervelocity penetration criteria for aluminum of reference 6, a thin-sheet effect factor of 1.5, assumed meteoroid impact velocity of 15 km/sec, and a ratio of aluminum penetrability to beryllium-copper penetrability of 2.0 (from ref. 1).

Figure 12 shows a discrepancy of several orders of magnitude between the penetration and impact data of the Explorer XVI. A similar, though not quite as

large, discrepancy is apparent between the Explorer XVI penetration data and the impact data collected by other spacecraft employing like impact detection systems, represented on figure 12 by the 1961 summary curve of Dubin, Alexander, and McCracken (ref. 5). No explanation is now available for the wide discrepancies in the results of these two experimental techniques. However, several factors can be listed as possible explanations of the observations. Some of these factors may be unique to the impact detection experiments of the Explorer XVI; others may be applicable to the microphone impact detection experimental technique in general. Factors probably unique to Explorer XVI include (a) possible degradation of the supporting electronics of the impact detection systems, particularly amplifier stages, due to the high-energy electron population in the Explorer XVI orbit; and (b) temperature effects upon the satellite structure (as distinguished from temperature effects upon the electronics package, which have been investigated and found negligible). Items (a) and (b) are further discussed in the following paragraphs.

The possibilities of detrimental effects upon the Explorer XVI electronic circuitries due to high electron energies and fluxes in its orbit were investigated prior to its launch. Calculations based upon the best information then available indicated that the components of Explorer XVI would be more than adequately protected by the shielding afforded to them by the satellite structural configuration. However, it was later found, after Explorer XVI was in orbit, that the electron population and energy in this region of space were much higher than estimated, and could have a detrimental effect. (An investigation to evaluate the effects of such electron bombardment on identical Explorer XVI electronic modules, post facto, is presently in process at the Langley Research Center.)

Study of the impact data of Explorer XVI appears to indicate a correlation between the temperature environment of portions of the satellite skin structure and impact activity, greater than what can be ascribed to chance or coincidence. Several reasons for the existence of such a correlation have been proposed, and are being investigated. These are related to variations of temperature gradients in the satellite skin structure and/or impact sensing transducer assemblies, variations of acoustic coupling factors, the seasonal variation of earth's shielding effect upon the satellite with earth's orbital position, subatomic particle irradiation, and so on; all of which may produce operating conditions very much different than the simulated environmental conditions imposed upon the satellite during its preflight qualification tests.

A characteristic of the Explorer XVI impact data is the high counting rates observed in the high- and low-sensitivity impact detection systems in the first few days of orbit, illustrated by figures 7, 8, and 11, and particularly evident in the high-sensitivity system, figure 7. Such an effect has been observed on a similar experiment on a satellite of this type (Explorer XIII, unpublished data) and on other satellite impact experiments, but the mechanism of the effect is not well understood. It is hypothesized that the initially high counting rates may be due to debris in the near vicinity of the satellite structure remaining from the ascent and injection into orbit, and which are temporarily loosely entrapped within the satellite structure; outgassing of elements of transducer arrays; thermal and/or mechanical strain relief "settling" effects; and so on.

A basic question with regard to the microphone-type impact experiments in general is the validity of the assumption that momentum response at hypervelocity meteoroid encounter is the same as, or even comparable with the observed momentum response of such systems at the low velocities employed for calibration.

POWER-SUPPLY-SYSTEM PERFORMANCE

Figure 13 is a simplified schematic diagram of each of the two power supply systems. Five solar-cell trays are connected through blocking diodes to the unregulated nominally 12-volt direct-current bus, and the battery is connected directly to the bus. The zener diodes are used to prevent excessive battery overcharging. The load current is approximately 10 milliamperes during standby and 200 milliamperes during transmission. The batteries supply all of the load current during darkness, and approximately 80 percent of the load during transmissions in sunlight. Both battery bus voltages were monitored by both telemeters.

An analysis of the telemetered values of battery voltages indicated that both power supply systems were functioning normally up to the time transmittal of usable data ceased. Figure 14 gives a history of the voltage readings of the battery in telemeter A for the 124 days (December 16, 1962, through April 19, 1963) that the system operated normally. Readings obtained approximately 24 hours apart during both sunlight and darkness transmissions (where available) are plotted. Also given are the percent deviations of the telemetered voltages from those predicted on the basis of preflight tests simulating the same orbital conditions determined for each interrogation. Figure 15 gives the same data for the battery in telemeter B for the 218 days (December 16, 1962, through July 22, 1963) this system functioned normally. Except for isolated cases discussed subsequently, the percent deviations from the expected voltages, for both power supplies, are within the error limits of the telemetry systems and the data handling methods. The absence of a downward trend indicates that there was no detectable battery deterioration, and that any solar-cell degradation was insufficient to affect the power supply performance. After telemeter A began to malfunction, the A battery voltages monitored by telemeter B indicated that the A power supply was still functioning normally as mentioned in a previous section.

A number of factors influenced the expected battery bus voltages. The factors that were considered when computing the percent deviations given in figures 14 and 15 are:

(1) Time in sunlight or darkness prior to interrogations. Figure 16 shows the variation of battery voltage during a simulated minimum-sunlit orbital cycle with one transmission in sunlight and one in darkness. The dotted line gives the voltage at the end of a 1-minute transmission. The sunlight voltage for the 15th day in figure 14 was unusually low because the satellite had been in sunlight less than 1 minute.

(2) The interval between the start of a transmission and the time the data sample was taken. Figure 17 gives expanded plots of the variation of battery

voltage during typical simulated interrogations in sunlight and in darkness. These periods were usually selected to come after the initial rapid voltage drop. When practical, the 5-second period began 10 seconds after the start of the transmission.

(3) Battery temperature (assumed to be same as telemetry temperature). Figure 18 shows the variation in end-of-interrogation battery voltages with temperature for simulated interrogations 46 minutes after the start of the sunlight period and 28 minutes after the start of the darkness period (see fig. 16). The highest battery temperatures and lowest battery voltages occurred during the two 100-percent sun periods encountered - beginning the 52d and 165th days.

Only one interrogation per orbit was assumed in this analysis. The batteries recovered rapidly after interrogations in sunlight, but more than one transmission per orbit could result in voltages lower than predicted. For example, the unusually low B battery voltage (in sunlight) indicated in figure 15 for the 211th day was recorded while the satellite telemetry was reported to be intermittently transmitting without being interrogated.

TEMPERATURES

Temperatures on Explorer XVI through July 22, 1963, continued essentially within the same ranges and had the same characteristics as shown in the temperature histories presented in reference 3. They remained well within acceptable limits and agreed closely with prelaunch estimates. The satellite experienced its second 100-percent sunlit period between May 29, 1963, and June 12, 1963, a period of slightly more than 13 days. Temperatures of the various components during this 100-percent sunlit period stabilized at somewhat lower values than during the satellite's first such period. This reduction was expected, since the position of the sun relative to the axis of rotation of the satellite had changed because of the movement of the earth around the sun, resulting in less average satellite cross-sectional area normal to the sun's radiation.

Telemetry temperatures during the second 100-percent sunlit period stabilized at 40° C (104° F), which was within design limits and approximately 10° C lower than the temperatures encountered during the first 100-percent sunlit period. Telemeter A effectively failed approximately 8 to 15 hours before the beginning of the second 100-percent sunlit period, when temperatures were only slightly less than 40° C. Since both telemeters performed during and after the first 100-percent sunlit period, and were ground tested at temperatures as high as 65° C (150° F) without malfunction, the elevated temperatures at the time of telemeter A failure are not considered to be the primary cause of failure. However, it is known that high temperatures can hasten the failure of an imperfect semiconductor component. Telemeter B failed on July 22, 1963, when the satellite was in 70-percent sunlight and the telemeter temperature was 22° C (72° F).

DATA REDUCTION

Transmission records were obtained during 908 separate orbits of the 3,005-orbit data lifetime of the Explorer XVI satellite. The recorded telemetry signals were processed at the Langley Research Center by means of an automatic pulse-duration-modulation--pulse-frequency-modulation (PDM-PFM) data readout system (see ref. 1) and an electronic data processing system.

Table V shows the volume of data reduced automatically. In general, it was necessary for the signal-to-noise ratio of the recorded telemetry signal to exceed 8 decibels in order for automatic data readout to be successful. In a limited number of cases, no signal was recorded for one of the two telemeters.

TABLE V

Orbits	Transmission records received	Total records processed	Number of Telemeter A records processed	Number of Telemeter B records processed
1 to 100	94	94	78	90
101 to 700	345	173	113	125
701 to 1,717	219	219	158	150
1,717 to 3,005	250	250	[a]27	166

[a]Reduced manually.

The table is divided into four periods. During the first 100 orbits the spacecraft telemeters were interrogated at least once during nearly every orbit. The frequency of interrogation was reduced during the second period (orbits 101 to 700). In addition, only half of these had to be processed in order to get all of the desired data.

Between the 1,717th and the 1,725th orbit, a component failure (see ref. 3) in telemeter A reduced the duration time of the frame synchronization channel by an amount that precluded further automatic readout of telemeter A. Subsequent data from this telemeter were reduced manually for a total of 27 interrogations. Pulse modulation of the telemeter A radio-frequency signal ceased after the 2,060th orbit. Automatic readout of data from telemeter B continued through the 3,005th orbit, after which pulse modulation of radio-frequency signal also ceased.

CONCLUSIONS

The Explorer XVI data discussed herein indicate the following conclusions:

1. Both of the Explorer XVI telemeter systems have ceased to transmit usable experimental data. Total failure of the first telemeter occurred on May 29, 1963, and total failure of the second telemeter occurred on July 22, 1963. The power supply systems were still operating satisfactorily when the telemeter failures occurred.

2. Through July 22, 1963, 44 punctures of the 0.001-inch-thick beryllium-copper pressure cells were recorded, yielding a puncture rate of 0.031 puncture/sq ft/day. With 95-percent confidence, the average puncture rate in 0.001-inch beryllium-copper lies between 0.041 and 0.022 puncture/sq ft/day.

3. Through July 22, 1963, there have been 11 punctures of the 0.002-inch-thick beryllium-copper pressurized cells, yielding a puncture rate of 0.016 puncture/sq ft/day. With 95-percent confidence, the average puncture rate in 0.002-inch beryllium-copper lies between 0.029 and 0.008 puncture/sq ft/day.

4. No punctures of the 0.005-inch-thick beryllium-copper pressurized cells have occurred through July 22, 1963. With 95-percent confidence the average puncture rate is no greater than 0.009 puncture/sq ft/day.

5. Puncture rates have not changed significantly from those determined through May 26, 1963. The values expressed in terms of equivalent thicknesses of aluminum continue to lie near the lower of the estimates derived from ground-based observations. They also continue to show a more gradual decrease of puncture rate with increasing skin thickness than previously estimated for this range of thicknesses.

6. One break of an 0.003-inch copper-wire card detector was indicated on June 28, 1963, and a break of an 0.002-inch copper-wire card detector was indicated on July 13, 1963.

7. Impact rates determined from the impact detection systems through April 19, 1963, are higher than those found in previous impact detector experiments. There appears to be a correlation between impact rates and rate of puncture of the pressurized cells.

8. Spacecraft temperatures through July 22, 1963, continued to remain within acceptable limits. Telemeter temperatures were within design limits when both failures occurred.

Langley Research Center,
National Aeronautics and Space Administration,
Langley Station, Hampton, Va., February 14, 1963.

REFERENCES

1. Hastings, Earl C., Jr., compiler: The Explorer XVI Micrometeoroid Satellite - Description and Preliminary Results for the Period December 16, 1962, Through January 13, 1963. NASA TM X-810, 1963.

2. Hastings, Earl C., Jr., compiler: The Explorer XVI Micrometeoroid Satellite - Supplement I, Preliminary Results for the Period January 14, 1963, Through March 2, 1963. NASA TM X-824, 1963.

3. Hastings, Earl C., Jr., compiler: The Explorer XVI Micrometeoroid Satellite - Supplement II, Preliminary Results for the Period March 3, 1963, Through May 26, 1963. NASA TM X-899, 1963.

4. Davidson, John R., and Sandorff, Paul E.: Environmental Problems of Space Flight Structures - II. Meteoroid Hazard. NASA TN D-1493, 1963.

5. McCracken, C. W., Alexander, W. M., and Dubin, M.: Direct Measurements of Interplanetary Dust Particles in the Vicinity of Earth. NASA TN D-1174, 1961.

6. Bjork, Robert L., and Gazley, Carl, Jr.: Estimated Damage to Space Vehicles by Meteoroids. U.S. Air Force Project RAND Res. Memo. RM-2332, The Rand Corp., Feb. 20. 1959.

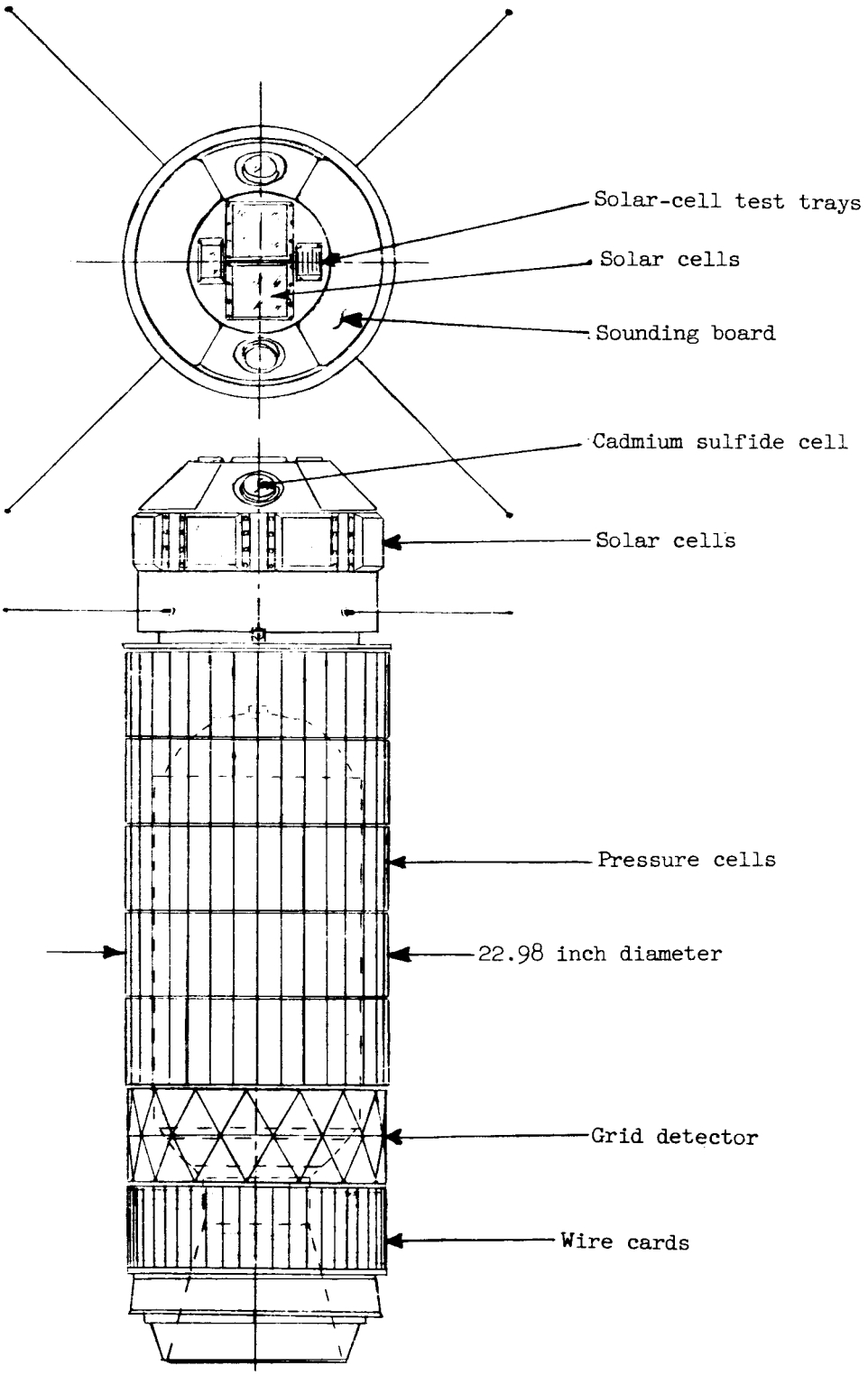

Figure 1.- Sketch of Explorer XVI showing locations of sensors.

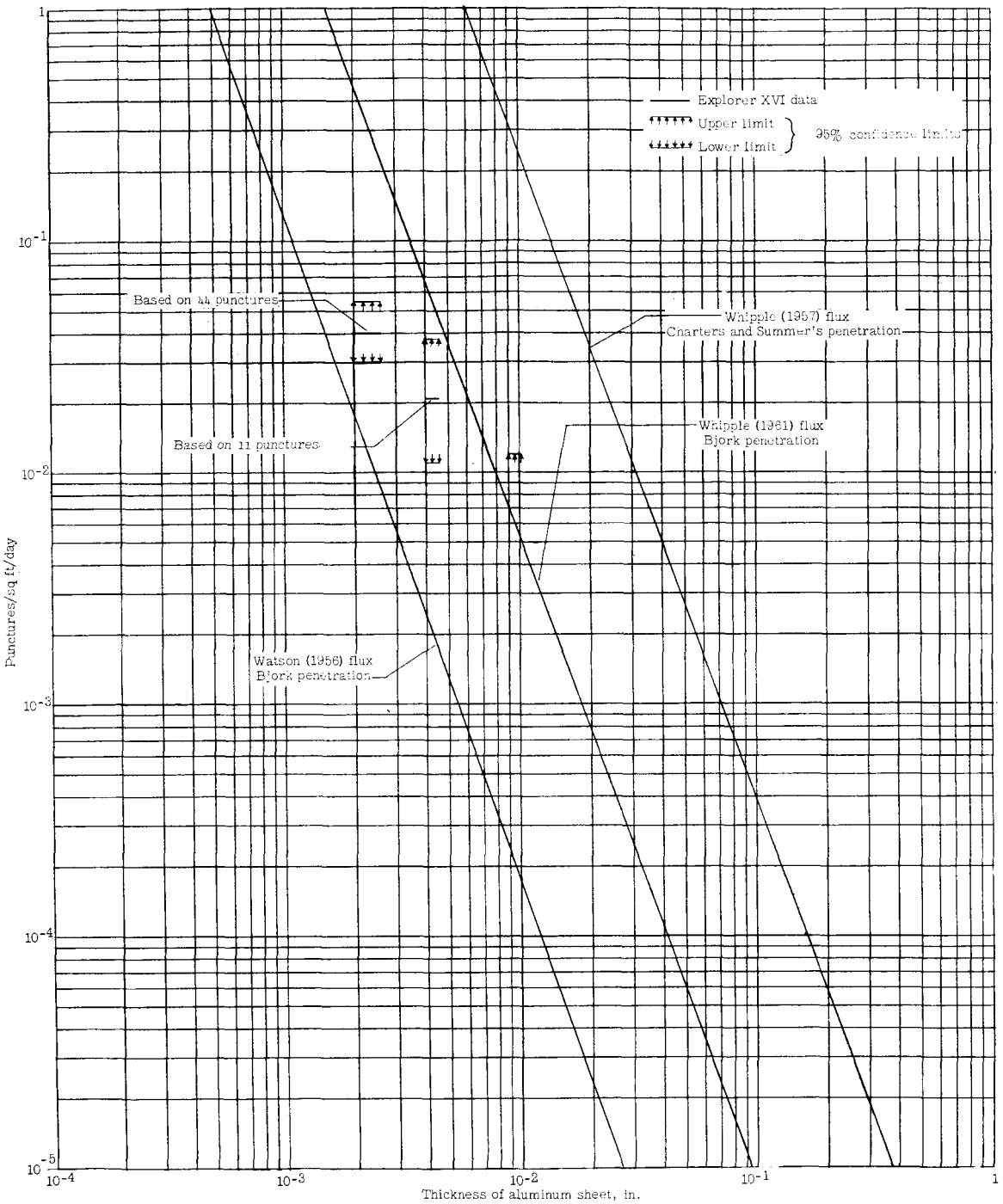

Figure 2.- Most probable rate of puncture of aluminum skin as a function of skin thickness, based on application of Bjork penetration theory to Whipple (1961) and Watson (1956) fluxes and Charters and Summers penetration theory to Whipple (1957) flux. Bars represent data from beryllium-copper pressure cells on Explorer XVI, as of July 22, 1963, tentatively interpreted in terms of aluminum with 95-percent confidence limits noted.

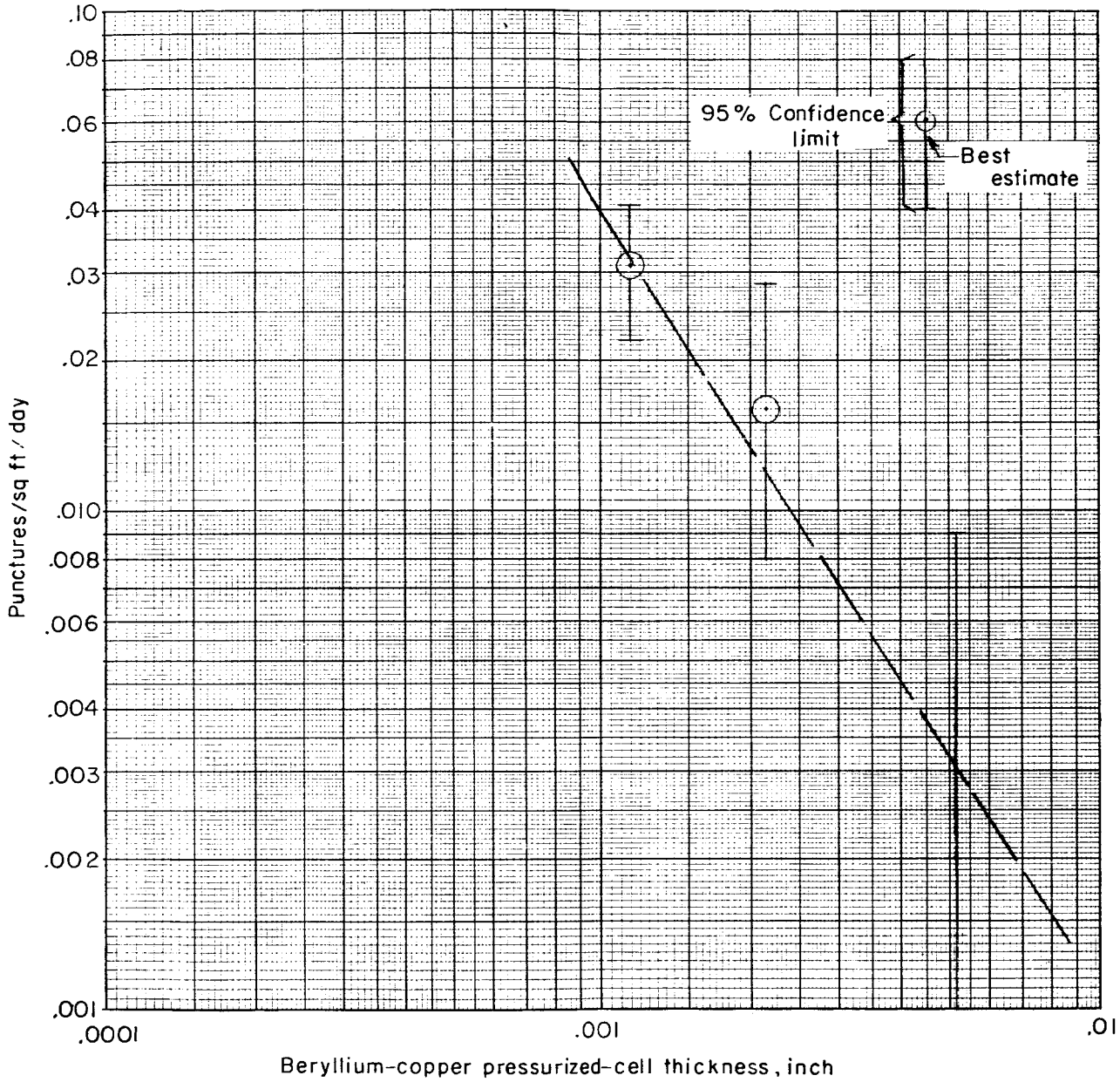

Figure 3.- Maximum-likelihood fit to data curve.

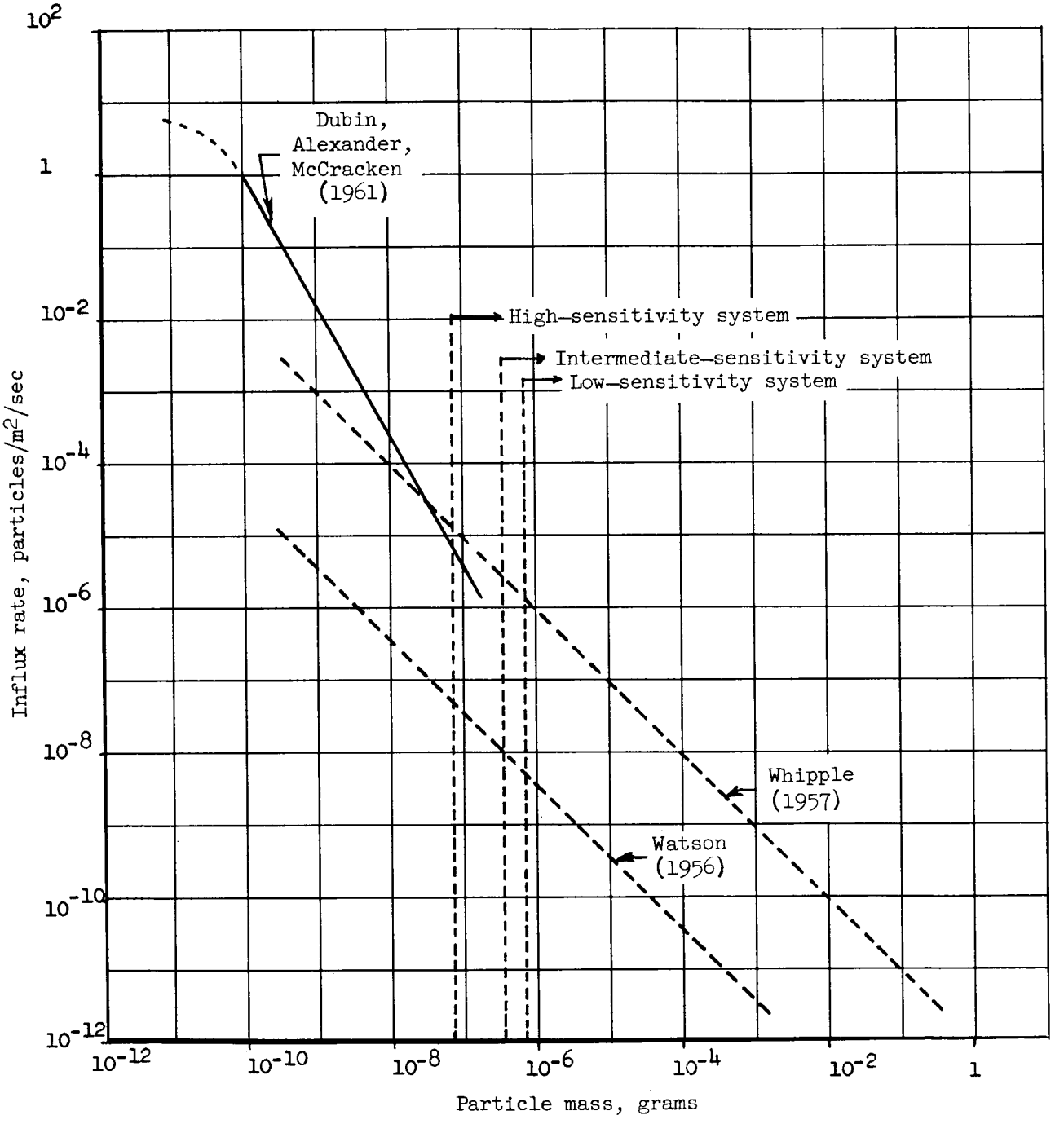

Figure 4.- Particle influx rate as a function of particle mass. (Assumed velocity is 15 km/sec.)

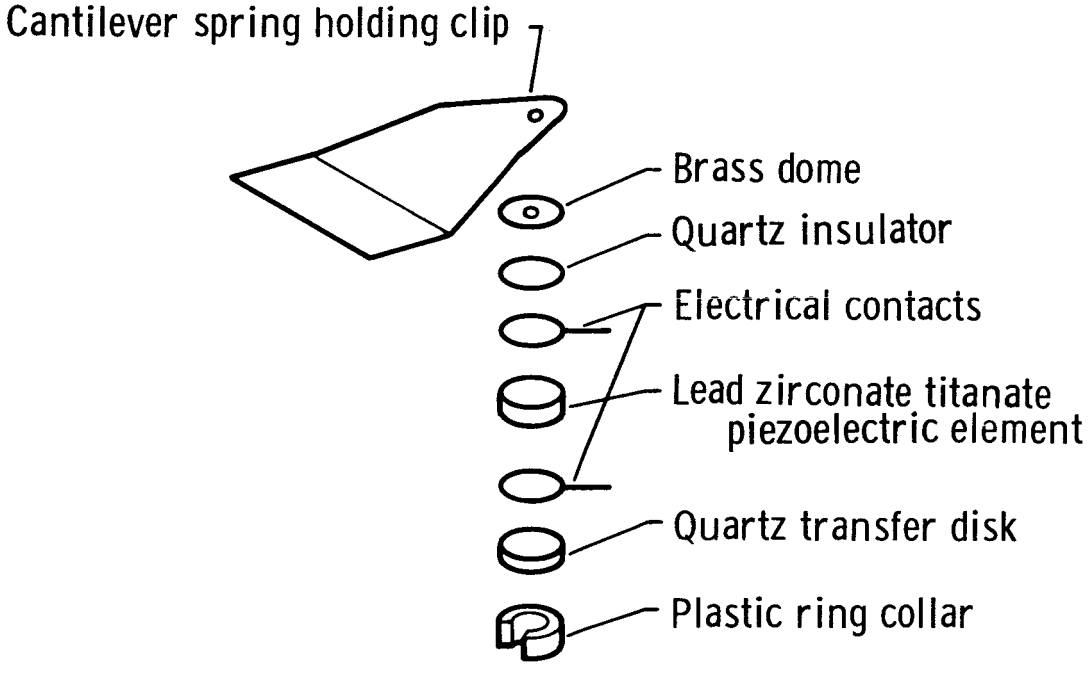

Figure 5.- Exploded view of piezoelectric impact-detector assembly.

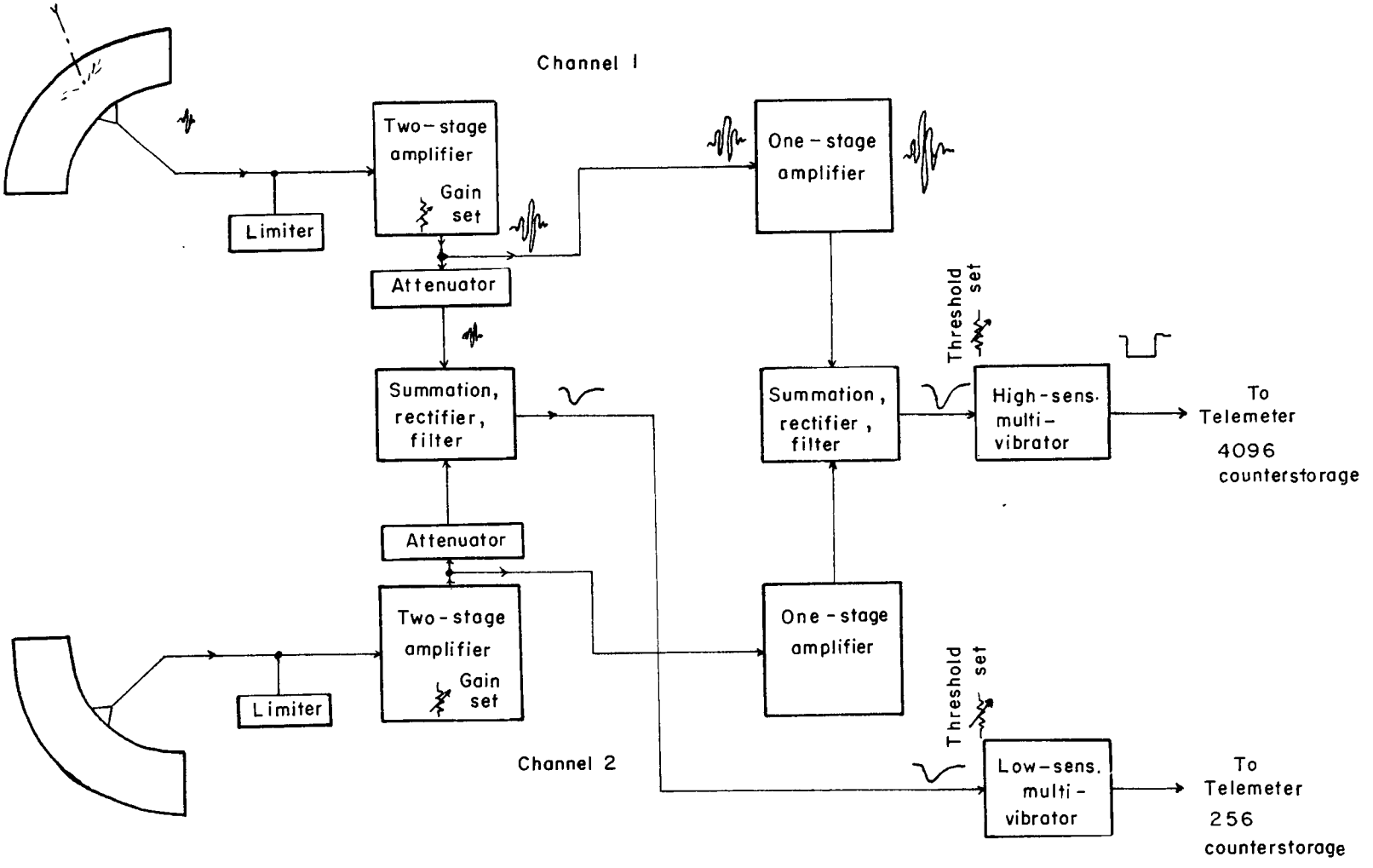

Figure 6.- Block diagram of impact-detector system.

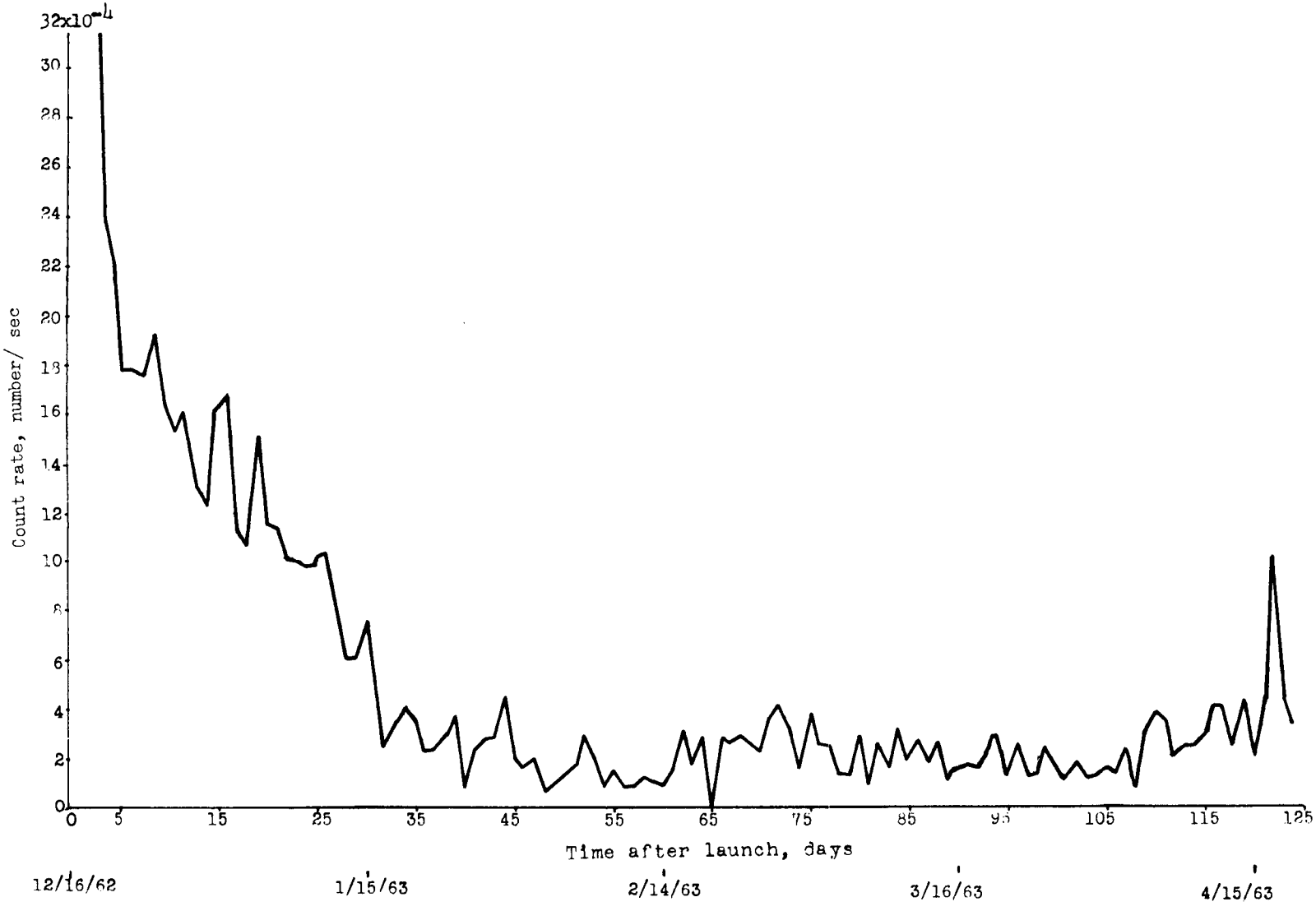

Figure 7.- Impact counting rate. High-sensitivity (0.1 dyne-sec) system; area, 0.142 square meter.

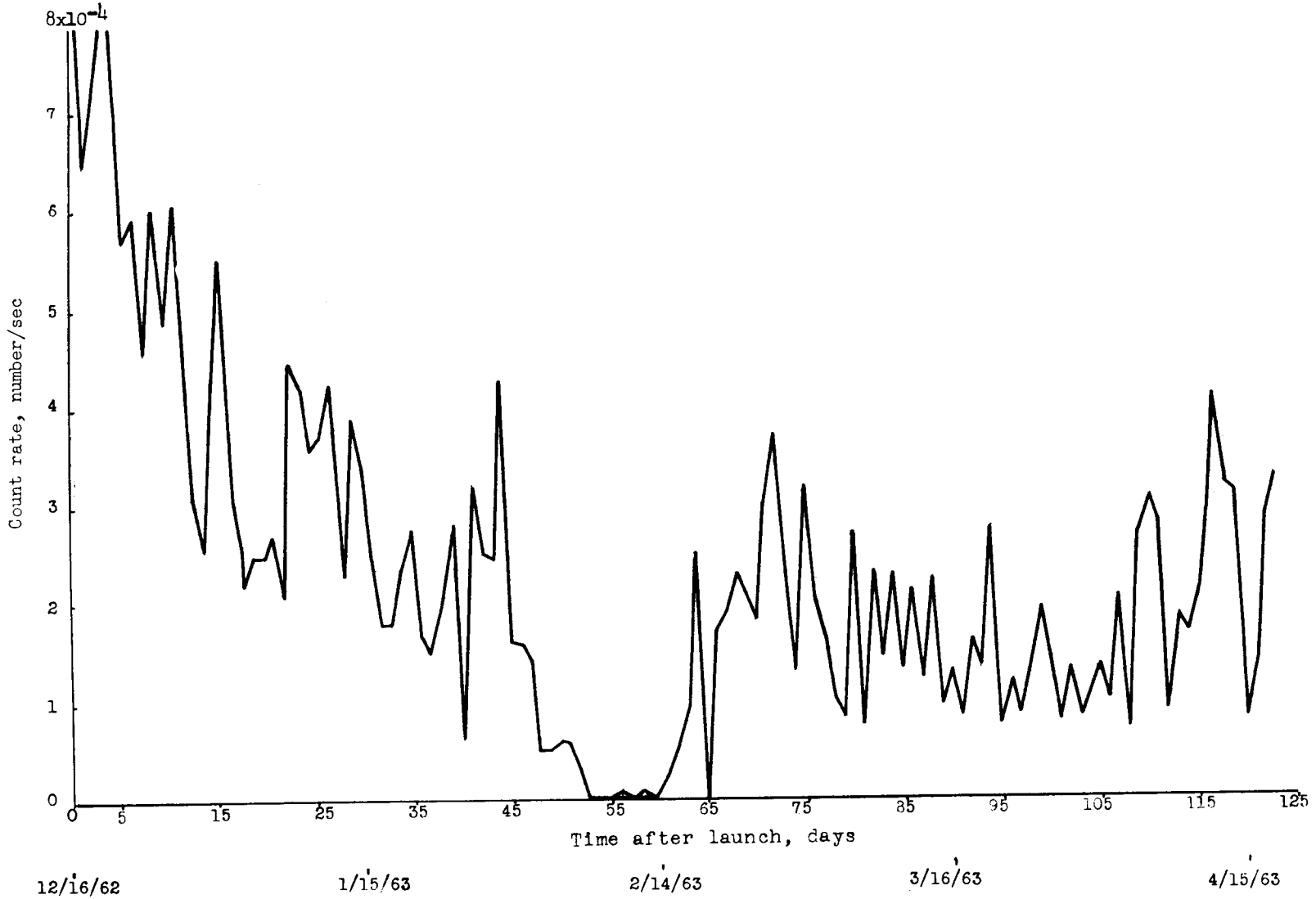

Figure 8.- Impact counting rate. Low-sensitivity (1.0 dyne-sec) system; area 0.142 square meter.

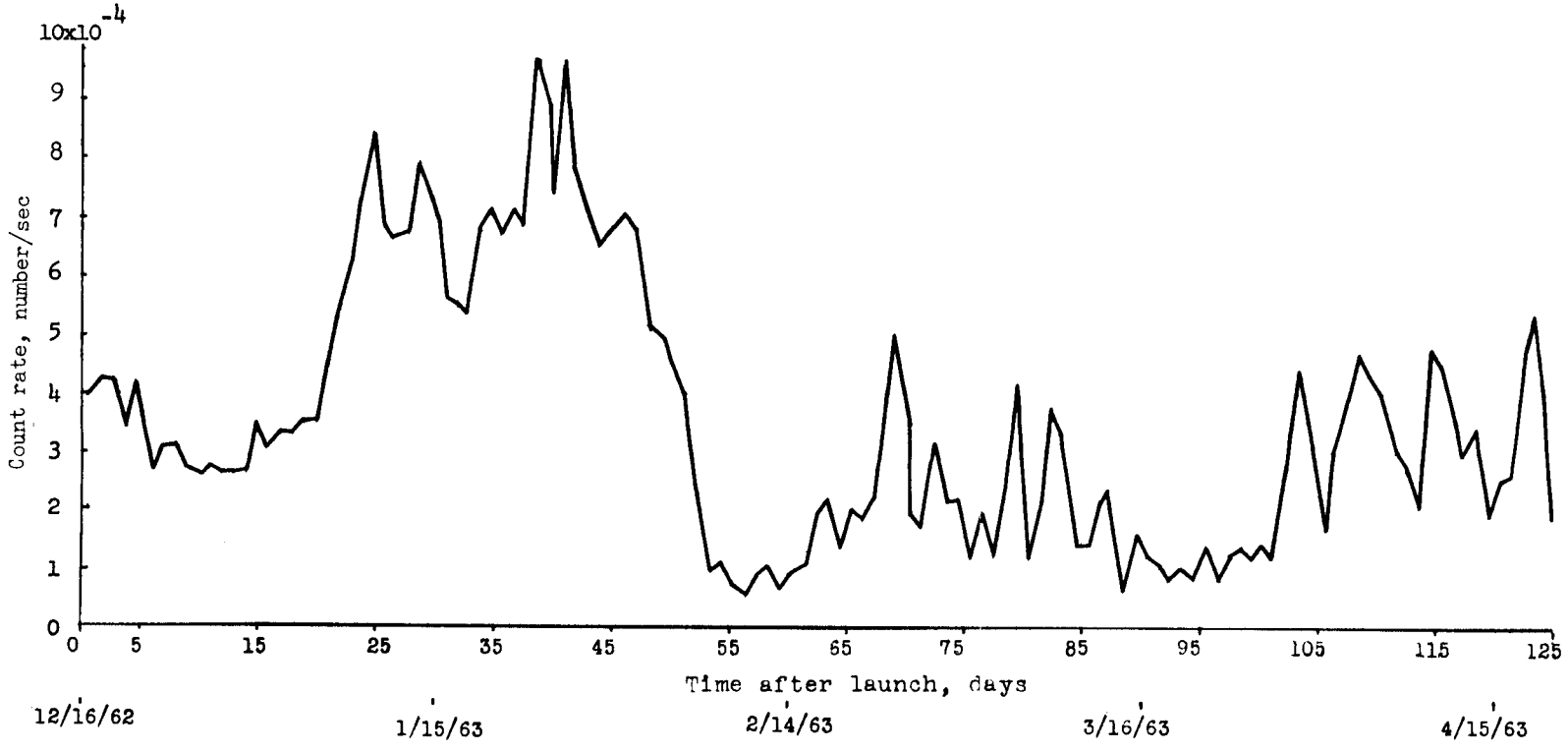

Figure 9.- Impact counting rate. Intermediate-sensitivity (0.5 dyne-sec) system; area, 0.186 square meter.

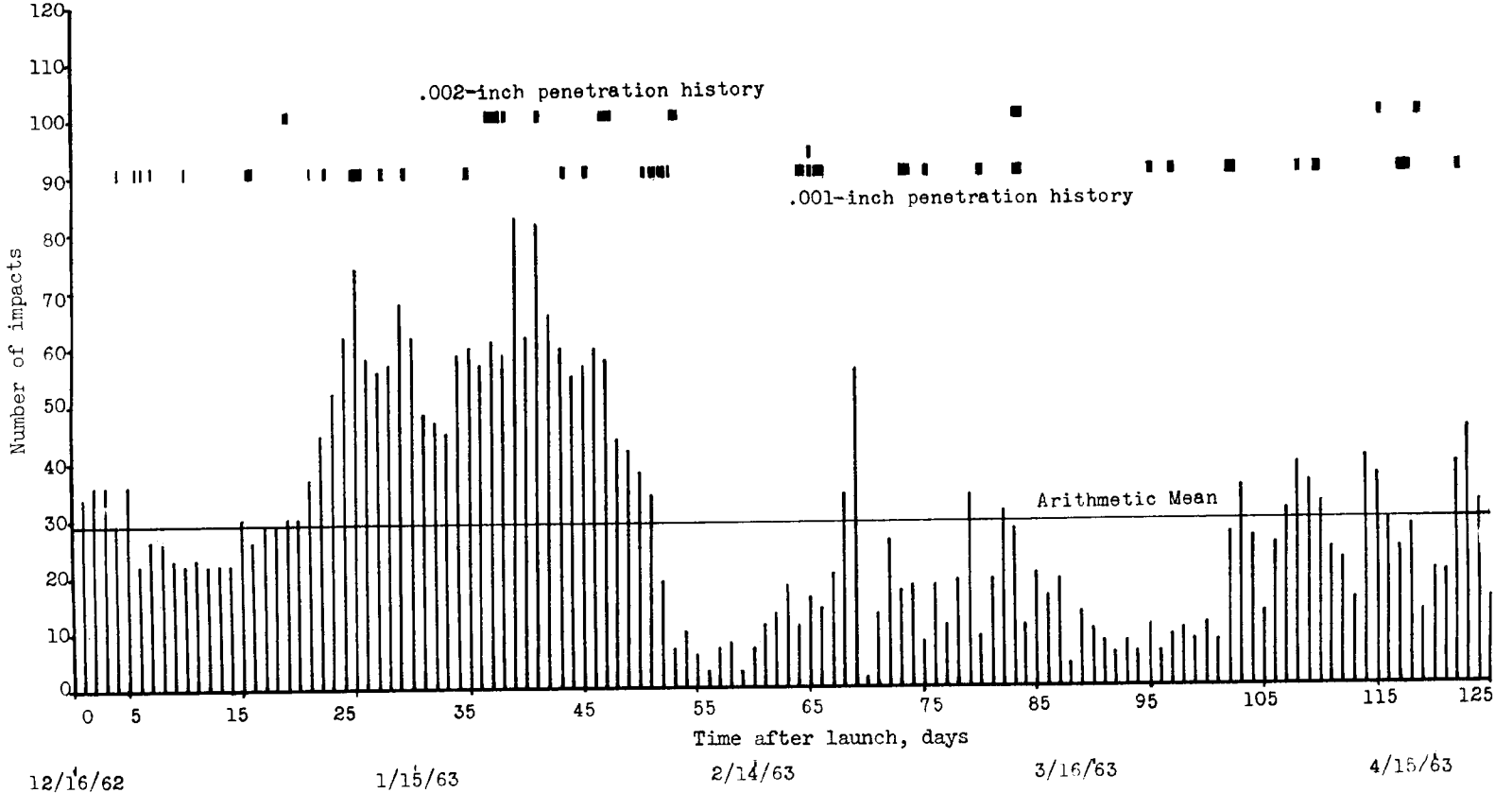

Figure 10.- Daily impact accumulation. Intermediate-sensitivity (0.5 dyne-sec) system; area, 0.186 square meter.

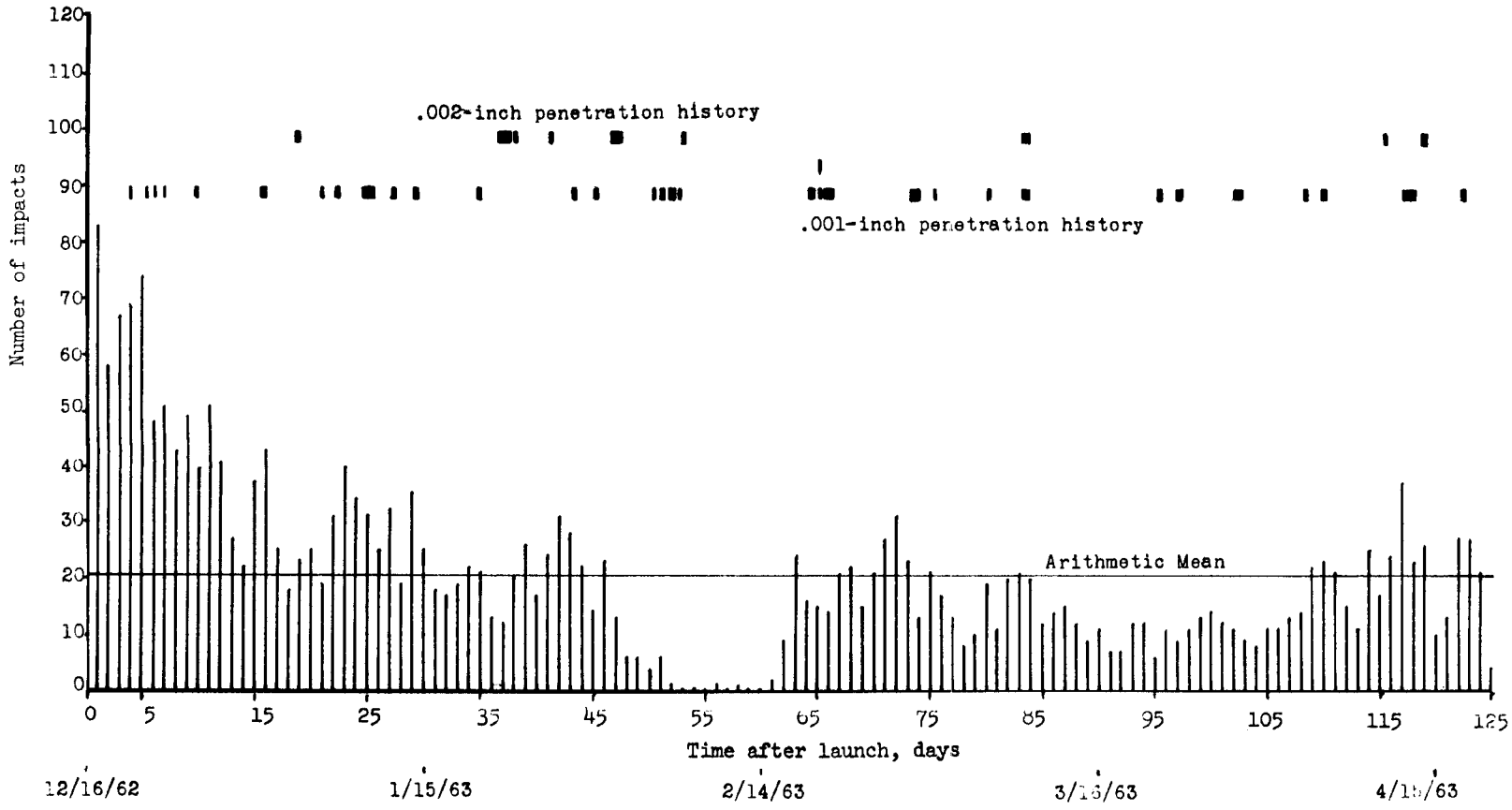

Figure 11.- Daily impact accumulation. Low-sensitivity (1.0 dyne-sec) system; area, 0.142 square meter.

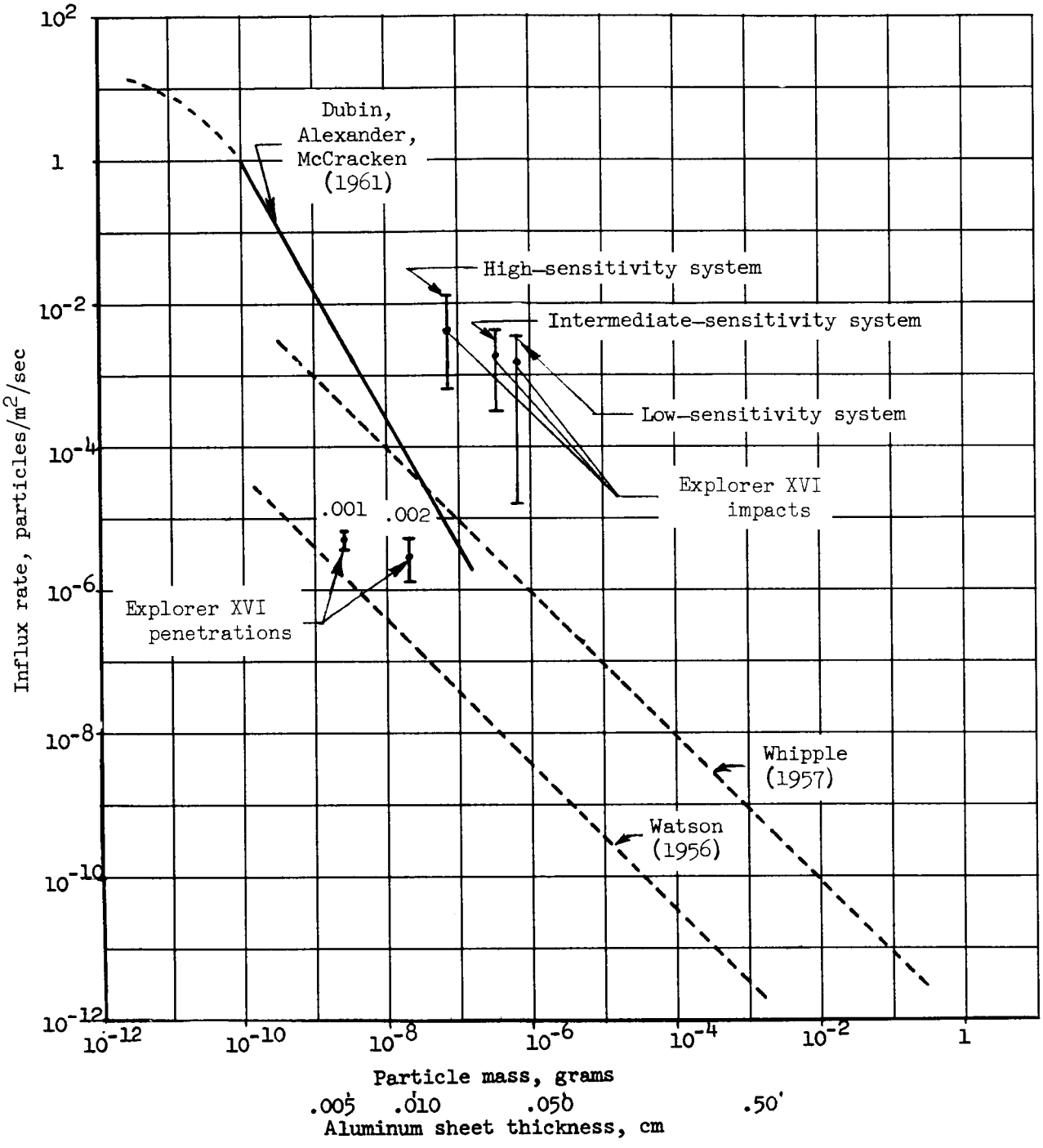

Figure 12.- Comparison of Explorer XVI influx-rate data with previous estimates. (Assumed impact velocity is 15 km/sec.)

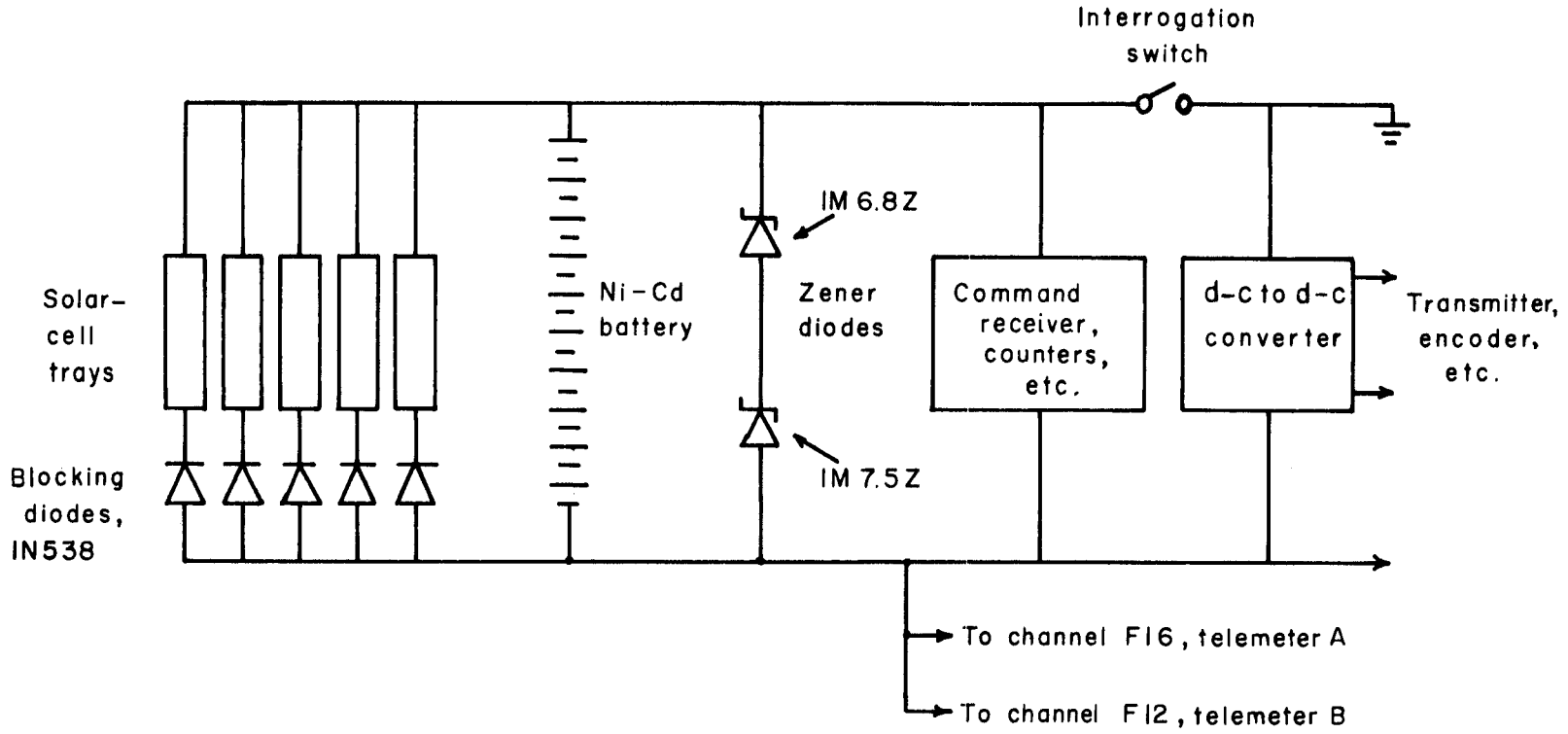

Figure 13.- Simplified schematic diagram of power supply for telemeter A.

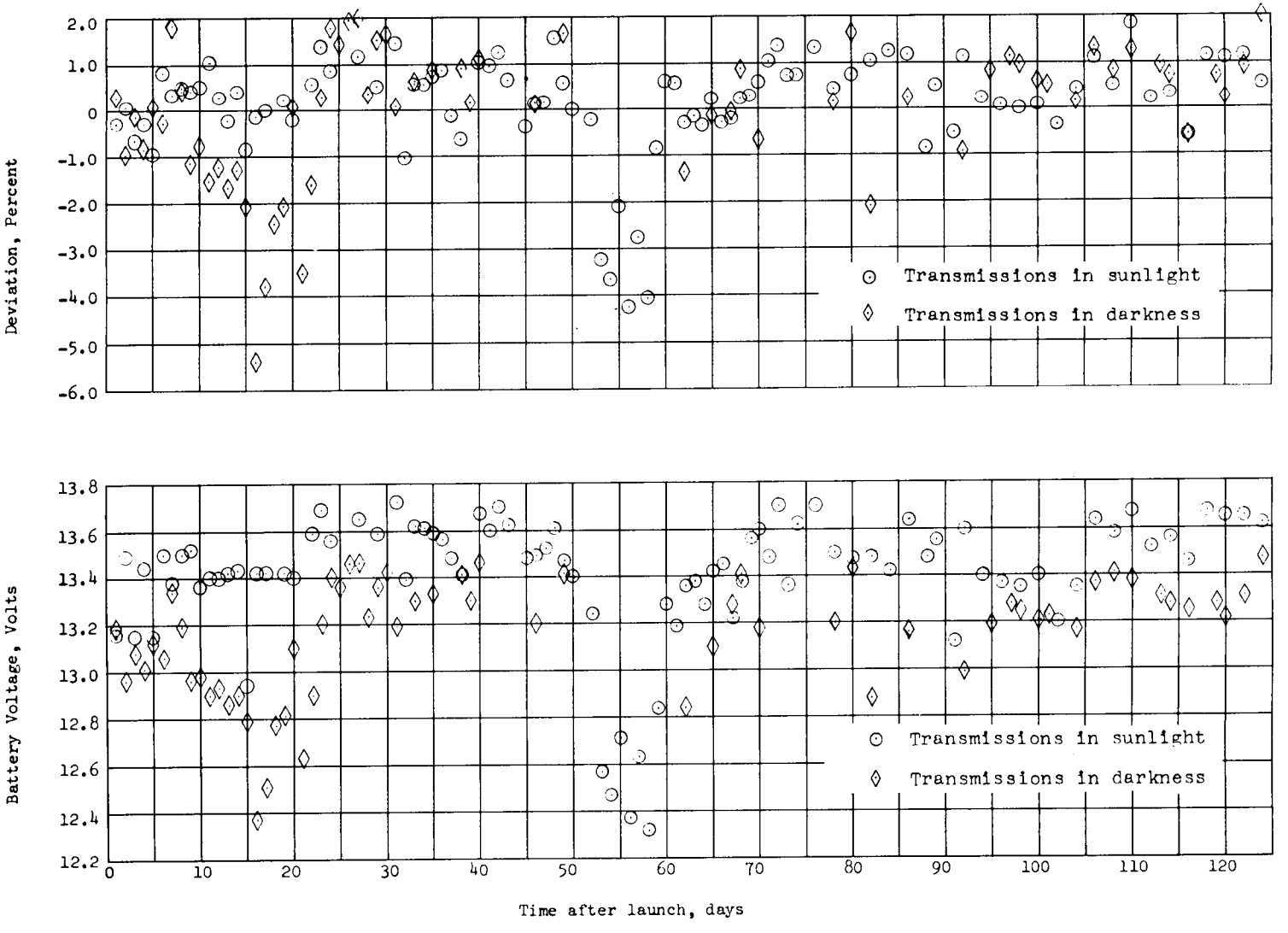

Figure 14.- Telemetered battery voltages from telemeter A and percent deviation of these voltages from those predicted on the basis of preflight tests.

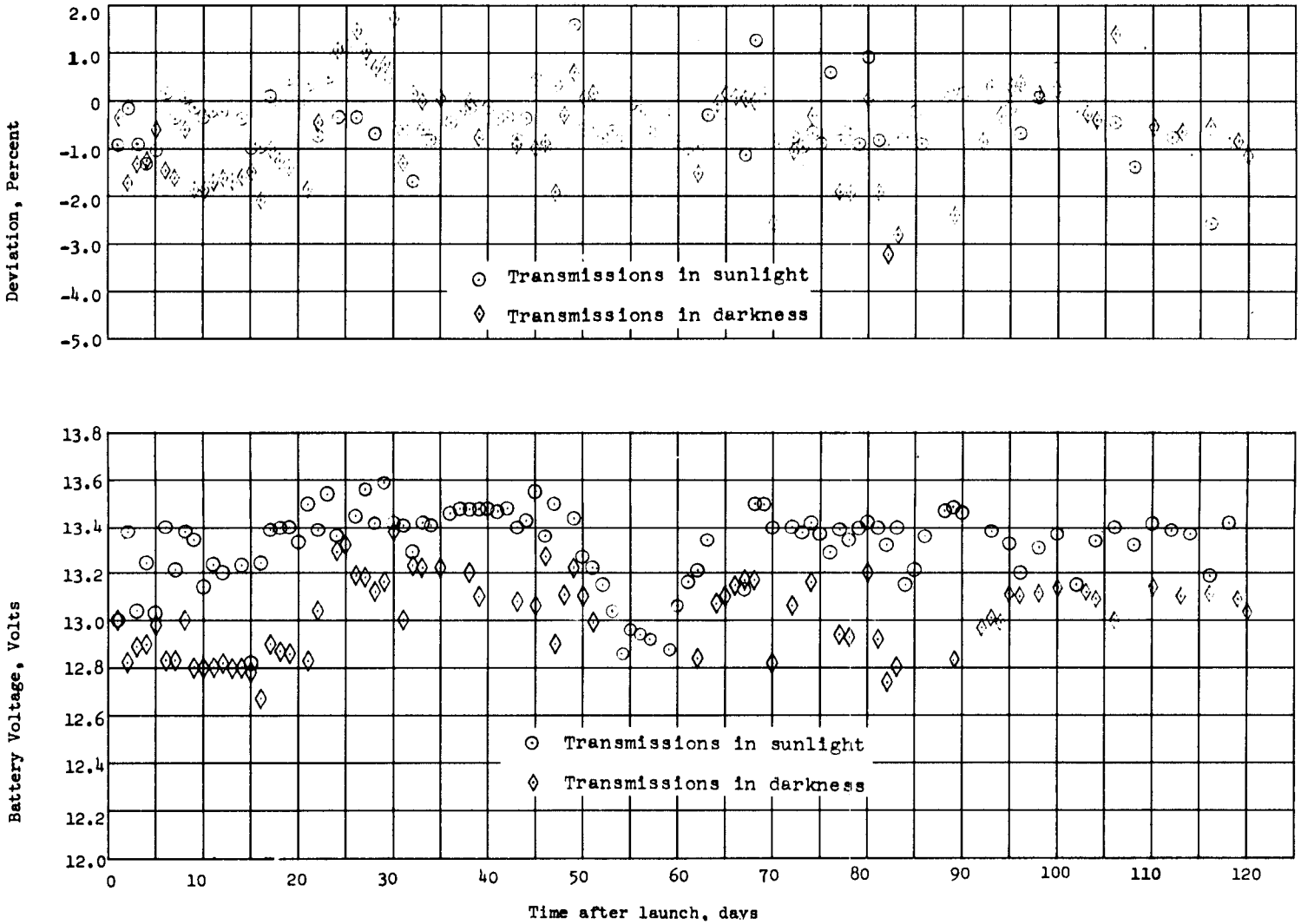

(a) 0 to 120 days after launch.

Figure 15.- Telemetered battery voltages from telemeter B and percent deviation of these voltages from those predicted on the basis of preflight tests.

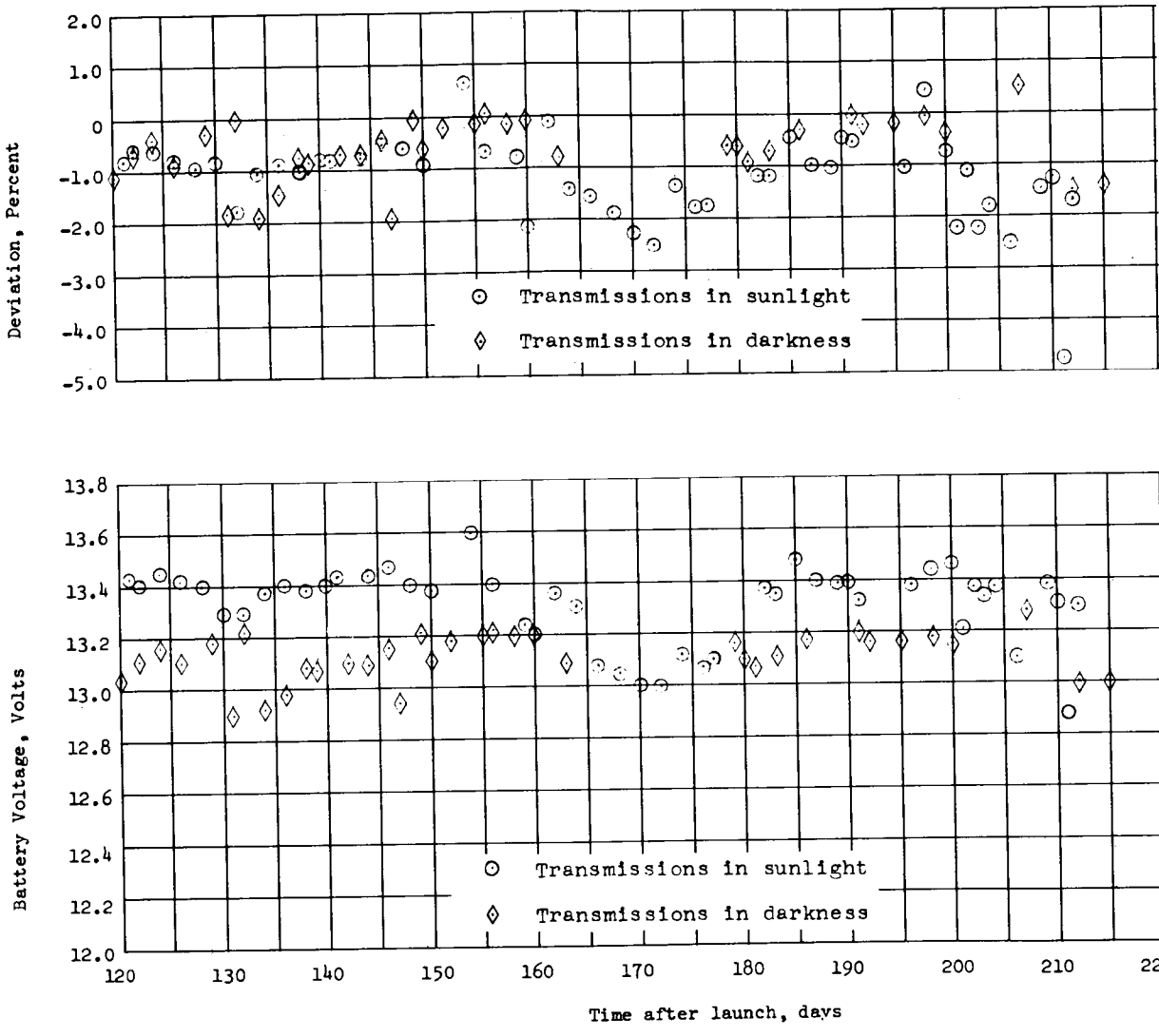

(b) 120 to 230 days after launch.

Figure 15.- Concluded.

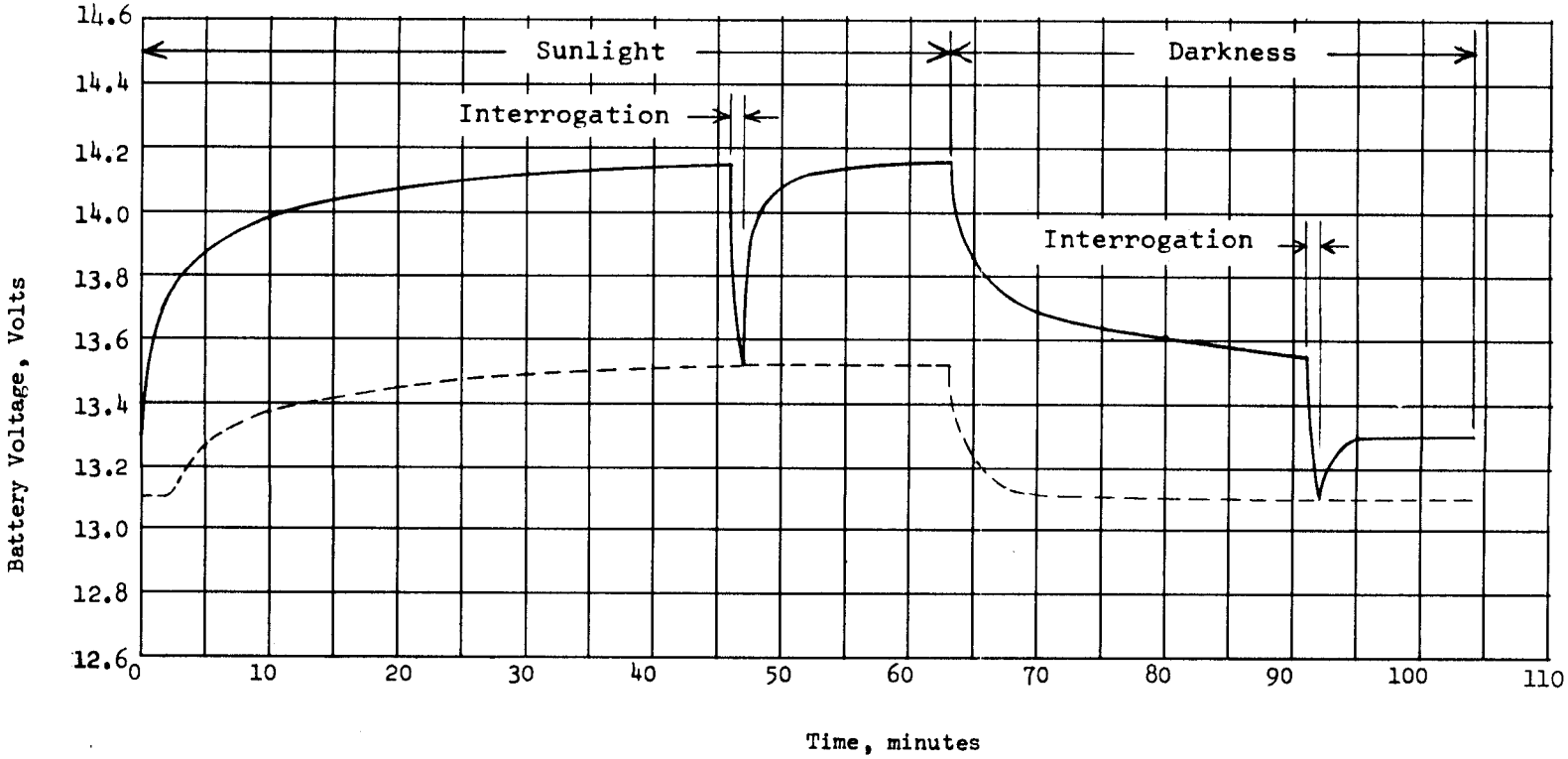

Figure 16.- Typical variation of battery voltage with time during simulated orbit, as measured in prelaunch cyclic tests of power supply. Typical effects of interrogations in sunlight and in darkness are shown. Dashed curve is locus voltage at end of interrogation. Temperature, 76° F.

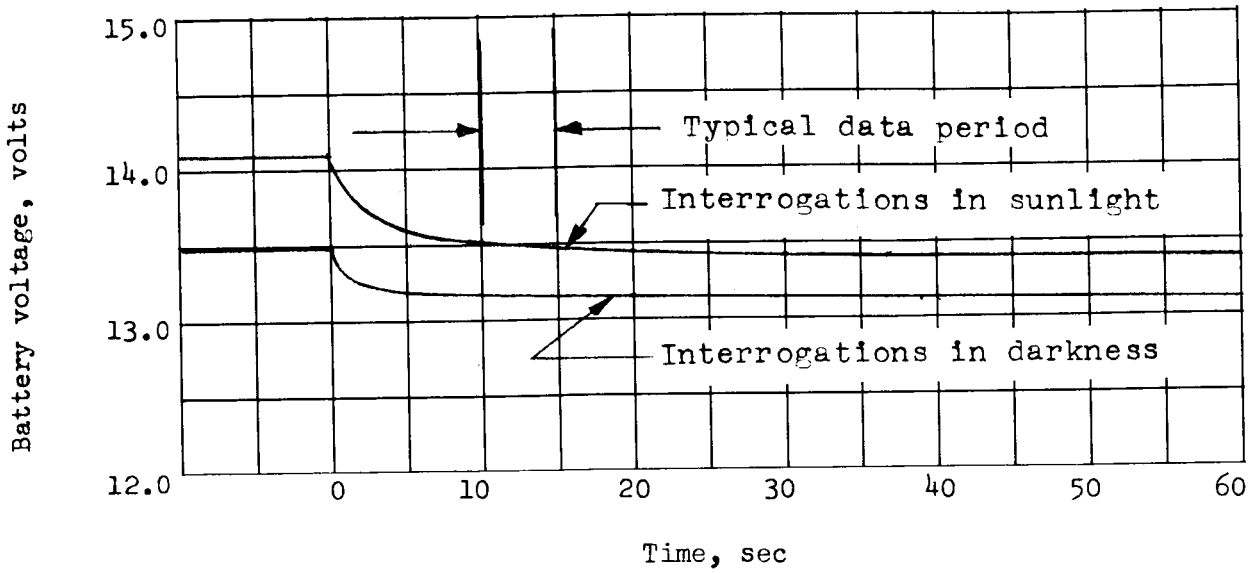

Figure 17.- Typical variation of battery voltage with time during an interrogation, as measured in simulated orbit during prelaunch cyclic tests of power supply. Temperature, 76° F.

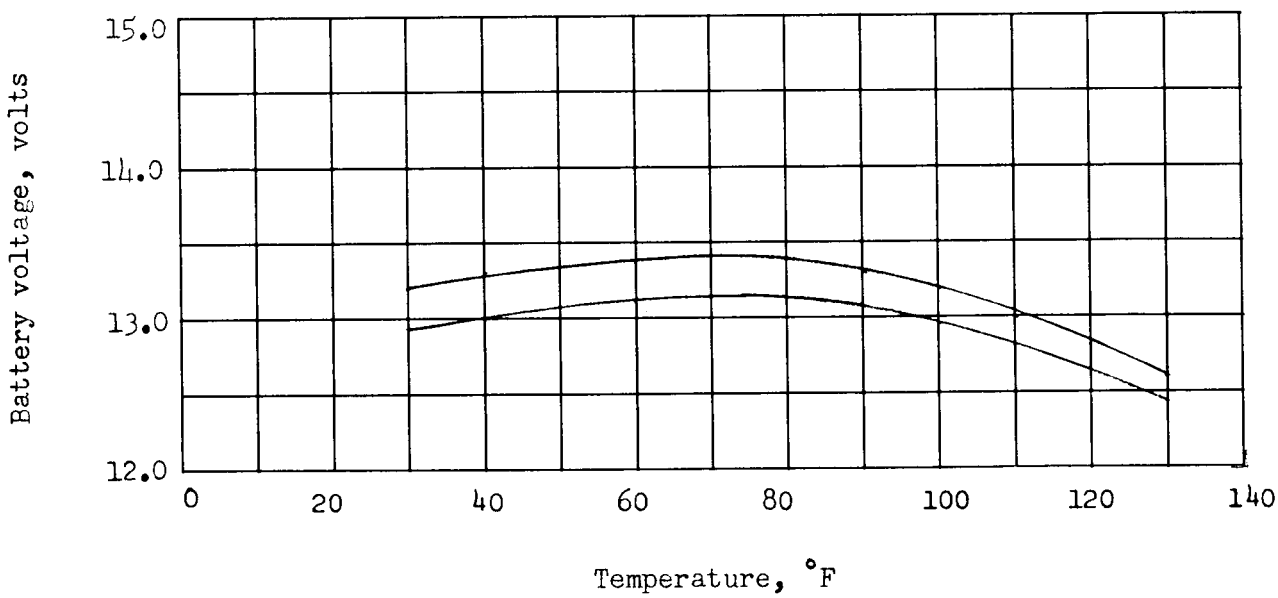

Figure 18.- Typical variations with temperatures of battery voltage at end of interrogation, as measured in simulated orbit during prelaunch cyclic tests of power supply.

NASA-Langley, 1964 L-3869